Chapter 1

Introduction

1.1 Narrow Linewidth Source for Fiber Lasers

1.1.1. The development of versatile fiber lasers sources

In general fiber-optic communication systems, fiber laser sources to serve as an optical channel must have narrow linewidth, high side-mode suppression ratio (at least > 35 dB), high stability, high output power, and low noise performance at fixed wavelength. With the fast evolution of Erbium-doped fiber amplifiers (EDFAs), narrow-linewidth and wavelength-tunable operation of such a high power optical source with wide gain spectrum has become an intriguing topic of researches for use in these communication systems and has received considerable attention recently. In particular, most efforts on the fiber laser, to date, have employed discrete optical components as part of the system to meet the aforementioned demands.

Previously, in order to obtain extremely narrow linewidth, versatile optical filters such as fiber Bragg gratings (FBGs) [1], tunable fiber Fabry-Perot etalons (FFPEs) [2], and other diffraction gratings have been emerged. However, these achievements are either complicated in fabrication or less cost-effective. Recently, novel external-feedback or self-seeding based filtering techniques for diode laser sources have been demonstrated [3]. Due to broadband spontaneous emission property and high output power of EDFAs, numerous researchers have been interested in building up wavelength-tunable and narrow-linewidth Er-doped fiber lasers (EDFLs) with filtering-characteristic passive devices and submodules. The most common and simple method to build up a narrow-linewidth EDFL source is by adding a

commercially available, intracavity optical band-pass filter (OBPF). Although this approach achieves wavelength-tuning simplicity, the SMSR and filtered linewidth of EDFL are still poor.

More recently, by using self-seeding with low-level (about 0.2~6%) feedback power of Fabry-Perot laser diode (FPLD), a low-cost and wavelength-tunable single-mode laser source has been demonstrated. Nearly single-mode pulses with SMSR of higher than 40 dB over a tuning range of 11.5 nm [4] were generated from the self-seeding FPLD. Nonetheless, this technique still relies on the use of a tunable linearly-chirped fiber Bragg grating to provide wavelength-selective feedback, and output filtering functions. Alternatively, the fast and wide-range wavelength tuning of FPLD can also be implemented via the provision of optical feedback into a self-seeded laser diode which also acts an active Fabry–Perot filter. By electrically tuning the comb-like spectral response of such an ordinary FPLD biased below its threshold, wavelength selection is realized and a stepwise wavelength tuning over a range of 9~11 nm with SMSR of from 13 to 22 dB throughout the range [5-7]. In particular, the power penalty caused during the self-seeding induced mode-selecting process is another disadvantage.

1.1.2. Mutual injection locking and mode beating noise

To release the predicament of the power dissipation and the finite SMSR performance of the self-seeded FPLD based filtering technique, a mutual injection locking between Fabry-Perot laser diode (FPLD) and close-loop regenerative EDFA amplification has been reported [8] to generate a high power, single-mode and ultrahigh SMSR. In a mutually injection-locked EDFL-FPLD link, a selected FPLD longitudinal mode is lasing with linewidth of <0.017 nm and SMSR of up to 50 dB [8].

Although the narrow-linewidth operation in EDFL-FPLD link is achieved, the lasing spectrum of the mutually injection-locked EDFL-FPLD link still includes significant beating noises due to dense longitudinal modes of long-cavity EDFL. The beating noise inevitably limits the application of the narrow-linewidth EDFL-FPLD link. To suppress the beating noise, an intra-cavity semiconductor optical amplifier based high-pass filtering technology has emerged [9, 10] recently.

1.1.3. Motivations for generating narrow linewidth and mode beating noise-free source

In order to obtain a narrow linewidth and mode beating noise-free laser source, we propose a new mutual injection-locked EDFA-FPLD link in this work. By using another optical band-pass filter before the FPLD and open the EDFL loop, side-mode suppression and further mode-beating noise elimination are achieved. Herein, the FPLD acts as a mode selector and an ultra-narrow band-pass filter. The difference of the optimized mutual injection-locking with the previous scheme is the use of an EDFA-FPLD link in which an open-loop EDFA is used to replace a close-loop EDFA (or EDFL) in previous demonstration. The proposed system further benefits from advantages including simplified setup, and high output power as compared with the conventional apparatus. The effect of FPLD current and the EDFA feedback power on the SMSR of the EDFA-amplified FPLD output is discussed. The performances of both configurations are also compared.

1.2 All-Optical Data Processing by Using Injection-Locked Lasers

1.2.1. Versatile NRZ-to-PRZ transformer by using FPLD

Recently, the Fabry-Perot laser diode (FPLD) based ultrafast all-optical signal processing systems are expected to play major roles in future all-optical networks (AONs) [11-16]. Versatile all-optical controlled signal processing techniques such as the clock frequency division [11,12], the wavelength conversion [13], the upstream traffic transmission [14], and nonreturn-to-zero- (NRZ-) to-pseudo-return-to-zero (PRZ) format transformation [15,16], have been demonstrated. To date, there are several methods reported to implement NRZ-to-PRZ transformation in FPLDs. Such a PRZ-format data can also be the potential candidate of carrier in a time-division multiplexing (TDM) system, which essentially helps to improve the bit rate and increase the network throughput. Chow *et al.* proposed an all-optical NRZ-to-PRZ format transformer structure, which is achieved by injection-locking a CW-lasing FPLD with a gain-switched pulse at one longitudinal mode of the FPLD, and concurrently seeding the FPLD with a optical pseudo-random binary sequence (PRBS) encoded data-stream at the another longitudinal mode of the FPLD [15].

Alternatively, Jeong *et al.* use transverse-magnetic (TM) mode absorption of an FPLD and the self-phase modulation (SPM) technique to achieve NRZ to PRZ data format conversion [16]. An FPLD has absorption nulls for a TM mode injected beam and the beam having NRZ data experiences SPM, which induces a frequency chirp at every rising edge and falling edge. By extracting the chirp components, all-optical NRZ-to-PRZ format conversion has been achieved. Therefore, using an FPLD to achieve all-optical data format transformation has become a very popular and potential

research.

1.2.2. Motivations for generating a simple NRZ-to-RZ data transformer

By taking the advantages of gain-switching and external injection-locking techniques, we propose a new NRZ-to-PRZ data conversion scheme by injecting a single-mode optical NRZ data into a synchronously modulated FPLD at unlasing condition. Unlike the previously reported methods, no additional DFBLD is required to achieve NRZ-to-PRZ operation in our case. Therefore, a lower-cost and simpler NRZ-to-PRZ transformer can be achieved. In contrast to previous approaches, the FPLD is operated without DC driving current, and is synchronously modulated by the RF clock signal with its maximum current equivalent to the threshold of the FPLD. The FPLD is neither lasing nor gain-switching in this case. When the FPLD is injected by an incoming optical NRZ data with high level (“1” bit), the threshold current of the FPLD is reduced and the gain-switching as well as the PRZ data-stream is generated from the FPLD. Such an external injection not only achieves the NRZ-to-PRZ transformation, but also helps to suppress the spontaneous emission and the gain of side modes. This eventually enhances the SMSR and reduces the noise level of the FPLD based data format transformer. Later on, the bit-error-rate (BER) and power penalty of this FPLD-based NRZ-to-PRZ transformer will be discussed.

1.3 The Introduction of Chapters

The thesis is separated into four chapters. Chapter 1 introduces versatile narrow linewidth source for fiber lasers, and all-optical data processing by using

injection-locked lasers. Chapter 2 describes mode beating noise suppression for mutually injection-locked Fabry-Perot laser diode and erbium-doped fiber amplifier link. Chapter 3 discusses all-optical NRZ-to-PRZ format transformer by injection-locking an Fabry-Perot laser diode at unlasing condition. At last, Chapter 4 concludes the experimental results and points out our future directions.

Chapter 2

Theory and Experiments of a Mode Beating Noise Suppressed and Mutually Injection-Locked Fabry-Perot Laser Diode and Erbium-Doped Fiber Amplifier Link

2.1 Abstract

By using Fabry-Perot laser diode (FPLD) as a resonant ultra-narrow band-pass filter in an Erbium-doped fiber amplified or laser (EDFA or EDFL), the theory and experiment for side-mode suppression and linewidth reduction of mutually injection-locked EDFL-FPLD and EDFA-FPLD links are demonstrated. Based on the amplified feedback injection loop, the 3-dB linewidth of 3.4 MHz for the EDFA-FPLD link is determined by using self-heterodyne interferometric spectral analysis. The EDFA-FPLD link exhibits a nearly mode-beating noise free performance as compared to the EDFL-FPLD link. This is due to the release of the resonant cavity configuration in the EDFL-FPLD link at a cost of slightly lower side-mode suppression ratio (~42 dB). The maximum output power of the EFDA-FPLD link is 20 mW under an FPLD input power of 0.1 mW.

2.2 Introduction

The mutually injection-locked semiconductor or fiber laser has received substantial attention [17-19] since which can produce a single longitudinal mode lasing with higher side mode suppression ratio (SMSR) for potential applications in the optical data communications. In principle, the injection locking laser systems strictly

rely on external seeding or self-feedback injection of a continuous-wave (CW) laser to achieve single mode and pulsed generation. Previously, a sampled grating distributed Bragg reflector laser CW lasing with SMSR of 30-50 dB and wide tuning range of 62 nm has been achieved [20]. In subsequent experiment, a DFB laser and Erbium-doped fiber laser were mutually injection-locked each other to achieve singly longitudinal-mode lasing, where the linewidth of the DFB laser is reduced to below 1.5 MHz [21]. On the other hand, various self-seeding and external seeding schemes were emerged to suppress the multi-mode spacing spectrum of a gain-switched Fabry-Perot Laser Diode (FPLD) [22], which enables single wavelength and wavelength-tunable operation of the FPLD pulses [23, 24]. In particular, the gain-switched FPLD is injected by the wavelength element from an external tunable laser source, and the single-mode optical pulses can be achieved when the injected wavelength coincides with one of the gain-switched FPLD modes. Later on, a dc-biased FPLD together with fiber Bragg grating has recently developed as the external-injection seeding source due to the high cost of the commonly used CW tunable laser source. However, the SMSR can be up to 42 dB but the wavelength tuning range is still narrow (about 11.5 nm) [25].

More recently, the mutual injection locking of an EDFL-FPLD link by low-level feedback injecting the fiber-pigtailed FPLD with an EDFL adapted from a commercial EDFA module was reported [8]. With the FPLD operating at just below its threshold condition (within 10% range), the EDFL-FPLD link can be lasing at a selected FPLD longitudinal mode with reduced linewidth of <0.017nm and an improved SMSR of up to 50 dB [26]. Nonetheless, the lasing spectrum of the mutually injection-locked EDFL-FPLD link still includes very many beating noises, which is produced by the dense longitudinal modes of EDFL with mode spacing of 4 MHz. Such a strong

beating noise in the narrow-linewidth EDFL-FPLD link puts severe limitations on its applications of the optical communication. To overcome this, L. Xu et al. have proposed to use a semiconductor optical amplifier in the laser cavity, which acts as a high-pass filter to suppress the beating noises in EDFL [10].

In this paper, we theoretically and experimentally analyze the linewidth reduction and SMSR improvement of an EDFL-FPLD link and EDFA-FPLD links by feedback seeding the FPLD using the EDFA in close- and open-loop configurations, respectively. The FPLD is acted as a mode selector and an ultra-narrow band-pass filter in such links. The optimized mutually injection-locking condition of the EDFA-FPLD link using an open-loop EDFA are compared with that using a close-loop EDFA (or EDFL) in previous demonstration. The performances of both configurations are discussed. We further demonstrate a side-mode elimination and mode-beating noise suppressing scheme by using an optical band-pass filter in the EDFA-FPLD link.

2.3 Experimental Setup

Prior to build up the EDFA-FPLD or EDFL-FPLD link, a bi-directionally 980 nm-pumped commercial Erbium-Doped Fiber Amplifier (EDFA) module with maximum output of 23 dBm is close-loop to form Erbium-Doped Fiber Laser (EDFL), as shown in Fig. 1(a). The EDFL-FPLD is constructed by using an FPLD in connection with a close-loop EDFA which functions as an EDFL with longitudinal mode spacing of only 4.4 MHz, as sown in Fig. 1(b). On the other hand, the EDFA-FPLD link denotes a similar system, in which the EDFA is not close-loop, as shown in Fig. 1(c). This design eliminates the generation and lasing of the EDFL longitudinal modes in the former EDFL-FPLD link. The EDFA-FPLD link is implemented only by use of optical couplers (OCs) with pre-determined power

splitting ratios, and in-line polarization controller (PC). Such a design excludes the use of other expansive components such as optical circulators, fiber Bragg gratings, DBR or DFB LDs. The wavelength, threshold current, and longitudinal mode spacing of the free-running FPLD at 35℃ are about 1560 nm, 12 mA and 1.2 nm, respectively. Two different mutual injection-locking links (EDFL-FPLD and EDFA-FPLD) are investigated in our experiments. In the EDFL-FPLD link [11] shown in Fig. 1(b), a 20% output from the EDFL is employed to externally seed the FPLD. This introduces an additional loss of about 1.1 dB. The OC2 (90:10) coupler avoids over-seeding of the FPLD and facilitates the smallest insertion loss of the FPLD when injecting into the EDFL. The OC3 with 50:50 coupling ratio combines the injection from FPLD and the 80% EDFL output to close-loop the EDFL. The length of the EDFL ring cavity is 45 m, which gives rise to a longitudinal mode spacing of 4.4 MHz (calculated by c/nL). Although this arrangement achieves the optimal SMSR, it still suffers the disadvantage of beating noises due to the longitudinal modes of EDFL. Alternatively, the EDFA-FPLD link is proposed as an amplified feedback seeding scheme. This implementation is slightly different from the EDFL-FPLD link, in which an EDFA is not regeneratively feedback by itself, as shown in Fig. 1(c). In the EDFA-FPLD link, the filtered ASE of EDFA feedback-injects into the FPLD after passing through a commercially available optical band-pass filter (OBPF). The bandwidths of the OBPF at 3dB- and 10dB- decay are 1.38 nm and 2.94 nm, which are measured by using a gain-clamped EDFA based broadband amplified spontaneous emission source. The OBPF inserted between the FPLD and EDFA avoids the feedback injection of amplified FPLD side-modes (although they are small as compared to the principle lasing mode) from EDFA to FPLD. This also helps the suppression of the beating noise in EDFA-FPLD link. By setting the constant

temperature and current of the FPLD as 35^{o}C and 10 mA, the coupling ratio of OC1 was varied to obtain the single-mode lasing with optimized SMSR in the EDFA-FPLD link. Between the FPLD and the EDFL (or EDFA), an in-line PC is employed to fine tune the power injected into the FPLD. The FPLD is then controlled at just below threshold condition, and the feedback injected power from the EDFL or EDFA is carefully adjusted. The feedback from EDFL (or EDFA) and the cavity-loss of FPLD compromise to facilitate one longitudinal mode with improved SMSR lasing in FPLD. The output of FPLD then feedback injects the EDFL or EDFA to obtain a linewidth-reduced output each link. The optimized linewidth reduction is observed under the precise control on the feedback power for FPLD, while the other side-modes in EDFL-FPLD or EDFA-FPLD link are greatly suppressed during the gain competition process. The output of an EDFL-FPLD or EDFA-FPLD link is monitored by optical spectrum analyzer (OSA, Advantest Q8384) with 0.01-nm resolution and optical power meter (ILX Lightwave, OMM-6810B) with an OC of 90:10 coupling ratio. To measure the actual linewidth and the mode-beating noise, the self-heterodyne beating spectral output of the EDFL-FPLD or EDFA-FPLD link is monitored by electrical spectrum analyzer (ESA, Agilent HP8565E) in connection with an interferometer (Agilent HP11980A) and a high-gain optical receiver (BCP 320A), as shown in Fig. 2.1.

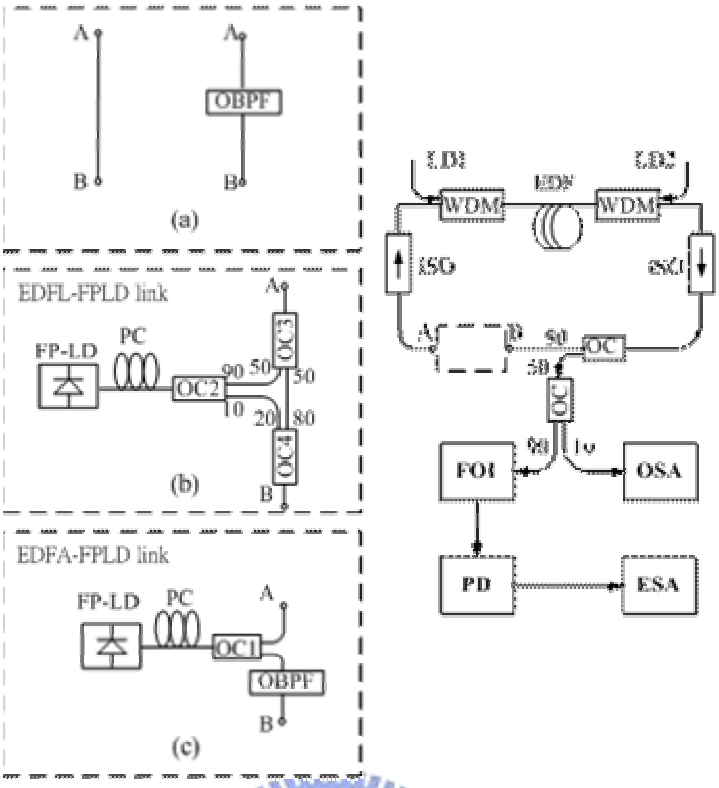

Fig. 2.1 The block diagrams of experimental setup. (a) the free-running EDFL without or with the OBPF (b) the configuration for an EDFL-FPLD link (c) the configuration for an EDFA-FPLD link PC: polarization controller; OC: optical coupler; OBPF: optical band-pass filter; WDM: wavelength division multiplexing; EDF: erbium-doped fiber; ISO: isolator; FOI: fiber-optic interferometer; PD: photo-detector; OSA: optical spectrum analyzer; ESA: electric spectrum analyzer.

2.4 Theoretical Simulation of SMSR and Linewidth

The principle of mutual injection-locking of the EDFA-FPLD (or EDFL-FPLD) has been elucidated in more detail. The FPLD is initially operated at below threshold condition, which is subsequently forced to be lasing by the feedback injection from EDFA (or EDFL). The FPLD is an intra-cavity component since the EDFA (or EDFL) and the FPLD are mutually injection-locked each other in the current setup (with a simplified block diagram shown as below). The lasing mode is decided by the FPLD instead of the EDFA (or EDFL). Remarkably, the linewidth and side-mode suppressing ratio of the EDFA-FPLD (or EDFL-FPLD) link is smaller than that of a

single FPLD at free-running condition. First of all, the SMSR of the FPLD without the feedback seeding from EDFA (or EDFL) is theoretically discussed. The optical fields of the principle and secondary (the largest side-mode) modes in the FPLD are denoted as E_1 and E_2, the time-dependent rate equation of the FPLD can be written as [27]:

$$\frac{d}{dt}[E_1 \exp(-j\omega t)] = [\frac{1}{2}(G_1 - \Gamma_1)]E_1 \exp(-j\omega t) + \frac{G_1 h\omega n_{sp}}{2\pi T_R}, \quad (2\text{-}1)$$

$$\frac{d}{dt}[E_2 \exp(-j\omega t)] = [\frac{1}{2}(G_2 - \Gamma_2)]E_2 \exp(-j\omega t) + \frac{G_2 h\omega n_{sp}}{2\pi T_R}, \quad (2\text{-}2)$$

In these equations, the index j define each parameter for the principle (j=1), the secondary (j=2, the largest side-mode), and the external (or feedback) injection mode (j=3). The *w* is the angular frequency, G_j is the gain coefficient, Γ_j is the loss coefficients, *h* is the Planck's constant, n_{sp} is the photon number of spontaneous emission, and T_R is the photon lifetime. The terms of $\frac{G_1 h\omega n_{sp}}{2\pi T_R}$ and $\frac{G_2 h\omega n_{sp}}{2\pi T_R}$ are the corresponding spontaneous emission noises. Moreover, G_1 and G_2 are expressed as

$$G_1 = \frac{g_{linear1}}{1 + \frac{I_1}{I_S(1)}}, \quad (2\text{-}3)$$

$$G_2 = \frac{g_{linear2}}{1 + \frac{I_2}{I_S(2)}}, \quad (2\text{-}4)$$

where $g_{linearj}$ is the linear gain coefficient, I_j is the optical intensity, $I_s(j)$ is the saturation intensity. In addition, Γ_j is defined by

$$\Gamma_j = -\frac{\ln(R_{eff,j})}{2L}, \quad (2\text{-}5)$$

where L is the cavity length of the FPLD, and $R_{eff,j}$ is the effective reflectivity. The intensity-related rate equations can also be given by substituting parameter E with I using the following equations

$$I = E \cdot E^* = |E|^2 \quad , \tag{2-6}$$

$$\frac{dI}{dt} = \frac{d}{dt}[E \cdot E^*] = E \cdot \frac{d}{dt}[E^*] + E^* \cdot \frac{d}{dt}[E] \quad , \tag{2-7}$$

In this case, the Eqs. (2-1) and (2-2) become

$$\frac{d}{dt}[I_1] = (G_1 - \Gamma_1)I_1 + \frac{G_1 h\omega n_{sp}}{2\pi T_R} \quad , \tag{2-8}$$

$$\frac{d}{dt}[I_2] = (G_2 - \Gamma_2)I_2 + \frac{G_2 h\omega n_{sp}}{2\pi T_R} \quad , \tag{2-9}$$

Under thermal equilibrium, the mode intensity is stable and not temporally fluctuated, we have

$$\frac{d}{dt}[I_1] = (G_1 - \Gamma_1)I_1 + \frac{G_1 h\omega n_{sp}}{2\pi T_R} = 0 \quad , \tag{2-10}$$

$$\frac{d}{dt}[I_2] = (G_2 - \Gamma_2)I_2 + \frac{G_2 h\omega n_{sp}}{2\pi T_R} = 0 \quad , \tag{2-11}$$

If we consider a simple model for the mutually injection-locked EDFA-FPLD (or EDFL-FPLD) link as illustrated in Fig. 2.2, in which two of the independent laser sources are injection-locking each other via an optical coupler or circulator.

Fig. 2.2 The mutually injection seeding scheme between FPLD and filtered EDFL (or EDFA).

When the FPLD is feedback seeded by an EDFA or EDFL source of filtered lasing lineshape, the Eqs. (2-1) and (2-2) can be re-written as

$$\frac{d}{dt}\{E_1 \exp(-i\omega t)\} = [\frac{1}{2}(G_1 - \Gamma_1)]E_1 \exp(-i\omega t) + [\frac{1}{2}\rho_3 \xi_3 \Gamma_3]E_3 \exp[-i(\omega t - \theta)] + \frac{G_1 h\omega n_{sp}}{2\pi T_R} \quad , \tag{2-12}$$

$$\frac{d}{dt}\{E_2\exp(-i\omega t)\}=[\frac{1}{2}(G_2-\Gamma_2)]E_2\exp(-i\omega t)+[\frac{1}{2}\rho_3\xi_3\Gamma_3]E_3\exp[-i(\omega t-\theta)] + \frac{G_2h\omega n_{sp}}{2\pi T_R} \quad , \tag{2-13}$$

where, E_3 and Γ_3 are the optical field and loss coefficient for feedback injection. ρ_3 is the propagation loss. ξ_3 is the differential quantum efficiency for the light emitted from laser to the grating output coupler. θ is the phase delay. It is seen that the feedback seeding term $[\frac{1}{2}\rho_3\xi_3\Gamma_3]E_3\exp[-i(\omega t-\theta)]$ form the EDFA (or EDFL) has been added to above equations. The intensity-related rate equation of two-modes in FPLD are expressed

$$\frac{d}{dt}[I_1]=(G_1-\Gamma_1)I_1+\rho_3\xi_3\Gamma_3I_3+\frac{G_1h\omega n_{sp}}{2\pi T_R} \quad , \tag{2-14}$$

$$\frac{d}{dt}[I_2]=(G_2-\Gamma_2)I_2+\rho_3\xi_3\Gamma_3I_3+\frac{G_2h\omega n_{sp}}{2\pi T_R} \quad . \tag{2-15}$$

If only the intensities of λ_1 (the central wavelength of principle mode) and λ_2 (the central wavelength of secondary mode) in the feedback injection can contribute to the FPLD lasing modes at same wavelength, the Eqs. (2-14) and (2-15) can be simplified as

$$\frac{d}{dt}[I_1]=(G_1-\Gamma_1)I_1+\rho_1\xi_1\Gamma_1I_1+\frac{G_1h\omega n_{sp}}{2\pi T_R} \quad , \tag{2-16}$$

$$\frac{d}{dt}[I_2]=(G_2-\Gamma_2)I_2+\rho_2\xi_2\Gamma_2I_2+\frac{G_2h\omega n_{sp}}{2\pi T_R} \quad , \tag{2-17}$$

By setting $(1-\rho_1\xi_1)\Gamma_1=\Gamma_1^{'}$ and $(1-\rho_2\xi_2)\Gamma_2=\Gamma_2^{'}$, we have

$$\frac{d}{dt}[I_1]=[G_1-(1-\rho_1\xi_1)\Gamma_1]I_1+\frac{G_1h\omega n_{sp}}{2\pi T_R}=[G_1-\Gamma_1^{'}]I_1+\frac{G_1h\omega n_{sp}}{2\pi T_R} \quad , \tag{2-18}$$

$$\frac{d}{dt}[I_2] = [G_2 - (1-\rho_2\xi_2)\Gamma_2]I_2 + \frac{G_2 h\omega n_{sp}}{2\pi T_R} = [G_2 - \Gamma_2^{'}]I_2 + \frac{G_2 h\omega n_{sp}}{2\pi T_R}, \quad (2\text{-}19)$$

Therefore, the SMSR of FPLD with feedback (or external) seeding from EDFA or EDFL can be expressed as

$$SMSR = \frac{I_1}{I_2} = \frac{g_1}{(\Gamma_1^{'} - g_1)} \times \frac{(\Gamma_2^{'} - g_2)}{g_2} = \frac{\frac{g_l}{(1+\frac{I_1}{I_S(1)})}}{\Gamma_1^{'} - \frac{g_l}{(1+\frac{I_1}{I_S(1)})}} \times \frac{\Gamma_2^{'} - \frac{g_l}{(1+\frac{I_1}{I_S(2)})}}{\frac{g_l}{(1+\frac{I_1}{I_S(2)})}}, \quad (2\text{-}20)$$

where the saturation intensity I_S can be described as

$$I_S(x) = \left(I_x \times \frac{\Gamma_x I_x}{I_x + \frac{hf}{T_R}} \right) \Bigg/ \left(g_l - \frac{\Gamma_x I_x}{I_x + \frac{hf}{T_R}} \right), \quad (2\text{-}21)$$

Assuming the saturation of the principle and side modes are equivalent (i.e. $I_s(1) = I_s(2)$), the gain of FPLD is relatively comparable to the loss of FPLD cavity at threshold condition, the output power of FPLD is about 0.1 mW under the feedback injection of EDFA or EDFL, the cavity length (L) is 250 μm, the refractive index (n) is 3.5, and the photon lifetime (T_R) is 5.8 ps, the SMSR, I_1/I_2, can thus be describe as a function of the ratio of loss coefficients.

$$\frac{I_1}{I_2} = \frac{C_1(\Gamma_2^{'} - C_2\Gamma_1^{'})}{\Gamma_1^{'}} = \frac{C_1(1 - C_2\Gamma_1^{'}/\Gamma_2^{'})}{\Gamma_1^{'}/\Gamma_2^{'}} = \frac{C_1\left[1 - C_2 \ln\left(R_{eff,1}^{'}\right)/\ln\left(R_{eff,2}^{'}\right)\right]}{\ln\left(R_{eff,1}^{'}\right)/\ln\left(R_{eff,2}^{'}\right)}, \quad (2\text{-}22)$$

where C_1 and C_2 are constants.

Therefore, the SMSR of the FPLD under feedback injection condition (by taking Γ_2 as a constant) is shown in Fig. 2.3. It is obviously that the SMSR of FPLD can be up to 50 dB if the loss of the principle mode is far smaller that the side mode (i.e., Γ_1/Γ_2 is infinitely small). Therefore, the use of a self-feedback seeding for the FPLD (after passing through an external mode-selecting element) essentially helps to reduce

the Γ_1/Γ_2 and to increase the SMSR of the mutually injection-locked EDFA-FPLD link.

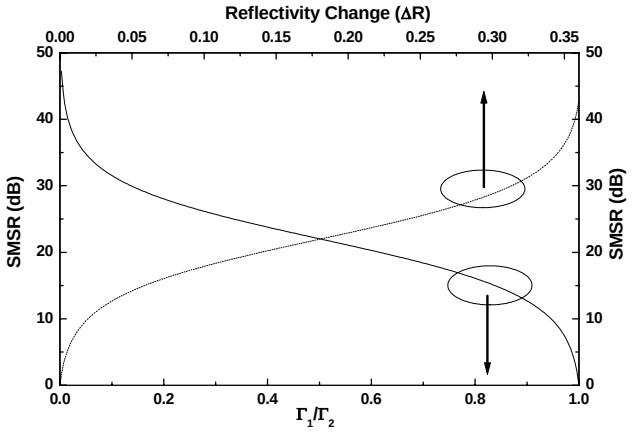

Fig. 2.3 The theoretically simulated SMSR of the mutually injection-locked EDFL-FPLD as function of reflectivity change (ΔR) and the ratio of loss coefficient (Γ_1/Γ_2).

In addition, the relationship between the loss coefficient Γ and the reflectivity R can be correlated each other by writing the following formula,

$$\Gamma_1 = -\frac{\ln(R'_{eff,1})}{2L}, \tag{2-23}$$

$$\Gamma_2 = -\frac{\ln(R'_{eff,2})}{2L}, \tag{2-24}$$

where $R'_{eff,j}$ denotes the effective reflectivity of the FPLD cavity under external feedback seeding from the EDFA or EDFL. Thus, the change of loss coefficient for the FPLD can thus be expressed as

$$\Delta\Gamma = -\frac{\partial}{\partial R}\left[\frac{\ln\left(R'_{eff}\right)}{2L}\right]\cdot\Delta R = -\frac{\Delta R}{2LR'_{eff}}, \tag{2-25}$$

The variation in loss coefficient of FPLD as a function of reflectivity change due to the feeding seeding of EDFA or EDFL is plotted in Fig. 2.4.

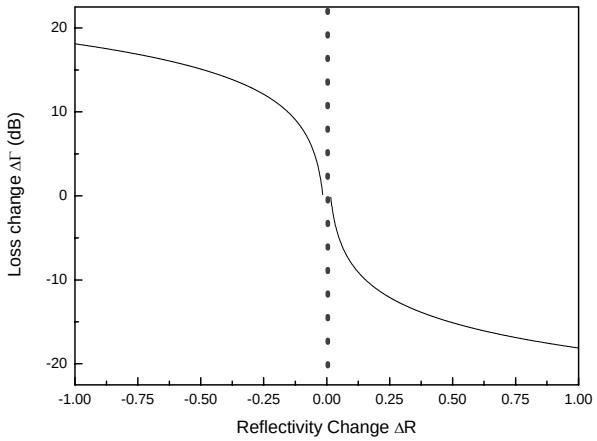

Fig. 2.4 The change of loss coefficient (ΔΓ) as a function of reflectivity change (ΔR) under the mutual injection-locking condition.

Consequently, the SMSR of FPLD under feedback injection condition can be re-written as a function of reflectivity change. The ratio of loss coefficients $\Gamma_1^{'}/\Gamma_2^{'}$ can be represented as

$$\frac{\Gamma_1'}{\Gamma_2'} \Rightarrow \frac{\Gamma_1+\Delta\Gamma_1}{\Gamma_2+\Delta\Gamma_2} = \frac{\Gamma_1-\dfrac{\Delta R}{2LR_{eff,1}}}{\Gamma_2-\dfrac{\Delta R}{2LR_{eff,2}}} = \frac{-\dfrac{\ln(R_{eff,1})}{2L}-\dfrac{\Delta R}{2LR_{eff,1}}}{-\dfrac{\ln(R_{eff,2})}{2L}-\dfrac{\Delta R}{2LR_{eff,2}}} = \frac{-\dfrac{1}{2L}[\ln(R_{eff,1}+\dfrac{\Delta R_{eff,1}}{R_{eff,1}})]}{-\dfrac{1}{2L}[\ln(R_{eff,2}+\dfrac{\Delta R_{eff,2}}{R_{eff,2}})]}, \qquad (2\text{-}26)$$

We assume that the effective reflectivity of the principle mode is equal to the largest side mode $R_{eff,1} \cong R_{eff,2} = \left(\dfrac{3.5-1}{3.5+1}\right)^2 = 0.31$, and the reflectivity change of the principle mode is far stronger to the largest side mode ($\Delta R_{eff,1} >> \Delta R_{eff,2} \approx 0$). The Eqs. (26) can be written as

$$\frac{\Gamma_1+\Delta\Gamma_1}{\Gamma_2+\Delta\Gamma_2} \cong \frac{[\ln(R_{eff,1}+\dfrac{\Delta R_{eff,1}}{R_{eff,1}})]}{[\ln(R_{eff,2})]}, \qquad (2\text{-}27)$$

Therefore, the SMSR of the FPLD as a function of reflectivity change due to the

feedback seeding from EDFA (or EDFL) can also be obtained (see Fig. 2.3).

Furthermore, with the feedback seeding from EDFA or EDFL, the linewidth of the FPLD is also evaluated. If we consider the Fabry-Perot etalon effect of the FPLD, the 3-dB linewidth of the FPLD lasing mode spectrum can thus be described as

$$\Delta\lambda = \frac{\lambda_1^2}{2\pi nL}\frac{(1-R_1G_1)}{\sqrt{R_1}\sqrt{G_1}}, \tag{2-28}$$

If the effective reflectivity of FPLD is slightly changed due to external feedback seeding, this may give rise to a change in the longitudinal-mode linewidth of FPLD. That is,

$$\Delta\lambda = \frac{\lambda_1^2}{2\pi nL}\frac{\left[1-R'_{eff,1}G_1\right]}{\sqrt{R'_{eff,1}}\sqrt{G_1}} = \frac{\lambda_1^2}{2\pi nL}\frac{\left[1-(R_1+\Delta R)G_1\right]}{\sqrt{(R_1+\Delta R)}\sqrt{G_1}}, \tag{2-29}$$

Thus, the simulated linewidth of the FPLD can also be plotted as a function of the change in reflectivity of the FPLD due to the feedback seeding of the EDFA or EDFL, as shown in Fig. 2.5. Therefore, the linewidth reduction and side-mode suppression of FPLD in the mutually injection-locked EDFA-FPLD link or EDFL-FPLD link can be understood through the theoretical modeling as shown above.

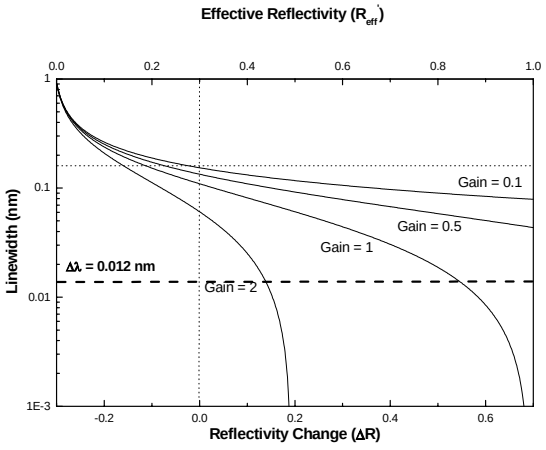

Fig. 2.5 The simulated linewidth of mutually injection-locked EDFL-FPLD link as a function of reflectivity change (ΔR).

2.5 Laser Linewidth Measurement

In this section, two methods for linewidth characterization of freerunning (unmodulated) singlemode lasers are discussed. Linewidth is often defined in terms of the fullwidth half-maximum (FWHM) of the optical field power spectrum. Grating based optical spectrum analyzers (OSAs) don't offer the measurement resolution required for laser linewidth measurement, so alternative characterization methods must be used. The alternative methods brought forth here include the optical heterodyne method and the delayed self-homodyne method. These methods are capable of obtaining the extremely high resolution required for laser linewidth measurements [28].

2.5.1 Heterodyne Using a Local Oscillator

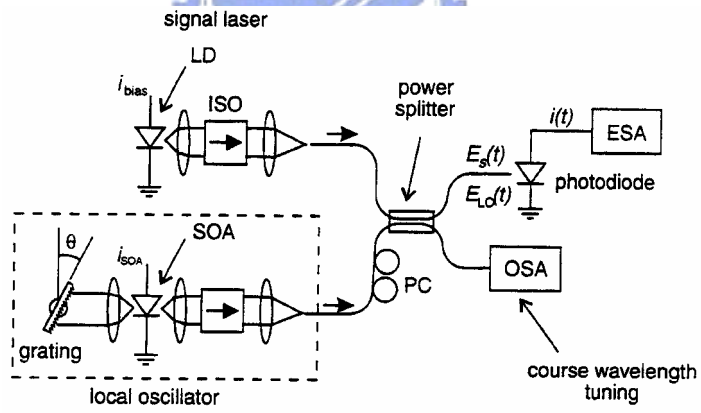

Fig. 2.6 Optical heterodyne setup for measuring laser linewidth using an external cavity laser for local oscillator. SOA = semiconductor optical amplifier, ISO = optical isolator, LD = semiconductor laser diode, PC = polarization state controller.

The setup for optical heterodyne discussed here is illustrated in Figure 2.6. In this setup, the reference laser (local oscillator with stable and narrow linewidth) is tuned appropriately and then its optical frequency is fixed during the measurement. This is possible because of the wide analysis bandwidth offered by electrical spectrum analyzers. An alternative way would be to have a narrow bandwidth electrical

detection and a swept local oscillator. This alternative method6 sets stringent requirements on the tuning fidelity of the local oscillator and will not be discussed further here. In Figure 2.6, light from the local oscillator (LO) is combined with the signal laser under test. A grating-tuned external cavity diode laser is used as the LO in this example. Polarization state converters are placed in the LO path to align the polarization state of the local oscillator to that of the signal under test. The coupler combines the two fields, delivering half the total power to each output port. One port leads to a photodetector which detects the interference beat tone, converting it to an electrical tone. Note that the local oscillator laser frequency must be tuned close to the signal laser frequency to allow the mixing product to fall within the bandwidth of typical detection electronics. A course alignment of the local oscillator wavelength is performed using an OSA or a wavelength meter. The local oscillator frequency is tuned to a frequency just lower than the average frequency of the laser under study. This creates a heterodyne beat tone between the LO and each of the frequency components in the signal spectrum as indicated in Figure 2.7.

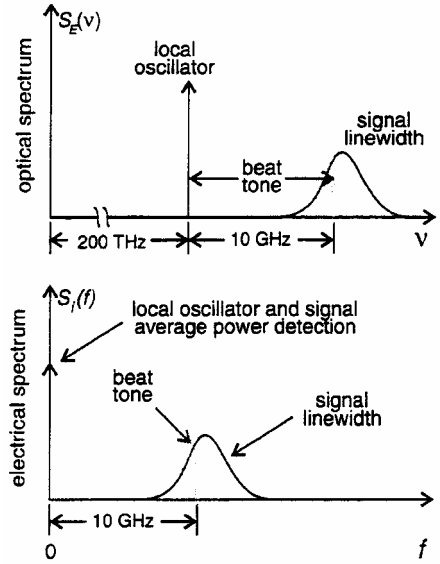

Fig. 2.7 The mixing process in terms of beat-tone slices mixed down to low frequencies that can be analyzed with electronic instrumentation.

Thus each frequency component is translated to a low-frequency interference term

described by:

$$i(t) = R\left[P_s(t) + P_{LO} + 2\sqrt{P_s(t)P_{LO}}\cos(2\pi(\upsilon_s - \upsilon_{LO})t + \Delta\phi(t))\right] \quad (2\text{-}30)$$

where ν_s and ν_{LO} are the frequencies of signal and local oscillator, P_s and P_{LO} are the powers for signal and local oscillator, R is the detector responsivity, and $\Delta\phi(t)$ is the time-varying phase difference. If the local-oscillator phase noise is small with respect to the test laser, the beat tone will be broadened primarily by the phase noise $\Delta\phi(t) \sim \phi_s(t)$ of the laser under study. The beat frequencies due to signal phase noise are measured using an ESA.

The ESA display is proportional to the power spectrum of the photodetector current which contains products of optical heterodyne mixing as well as direct detection terms.

$$S_i(f) \approx R^2\{S_d(f) + 2[S_{LO}(\upsilon) \otimes S_s(-\upsilon)]\} \quad (2\text{-}31)$$

(ESA = direct detection + heterodyne spectrum)

$S_d(f)$ is the ordinary direct detection that could be measured with just a photodetector and ESA. The second term is the useful heterodyne mixing product which is the convolution of the local oscillator spectrum $S_{LO}(v)$ with the signal spectrum $S_s(v)$. The convolution originates from the multiplication of the time-varying local oscillator field with the signal field in the photodetector. Multiplication in the time domain is equivalent to convolution in the frequency domain. The lineshape of the laser, including any asymmetries, is replicated at a low frequency set by the optical frequency difference between the two lasers. The convolution given in Equation (2-31) is illustrated in Figure 2.8. As the convolution scans the LO lineshape (Dirac-Δ function as shown) from negative infinity, it passes to zero at v_{LO}, traces out the test-laser lineshape and continues to positive infinity. The net result is a translation of the test-laser lineshape to the average difference frequency between the

LO and the test laser. Note from Equation (2-30) that as the LO linewidth broadens, its linewidth can dominate the photocurrent spectrum and decrease the frequency resolution of the heterodyne measurement.

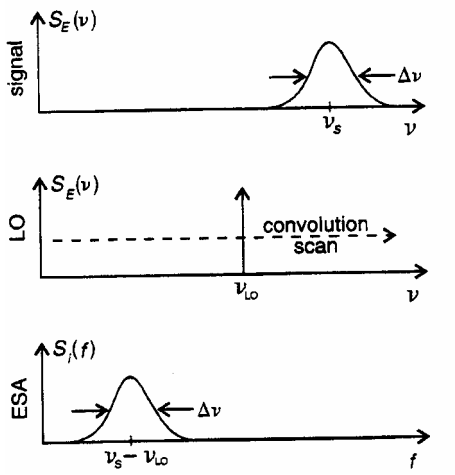

Fig. 2.8 Convolution of narrow linewidth laser translates signal spectrum to low frequencies.

If the LO laser linewidth is small compared to the laser under test, the lineshape spectrum of the local oscillator, $S_{LO}(\nu)$ is approximated with a Dirac-Δ function: $P_{LO}\,\delta(\nu - \nu LO)$. Thus from Equation (2-31) the ESA will display:

$$S_i(f) \approx 2R^2 P_{LO} S_s(\upsilon - \upsilon_{LO}) \tag{2.32}$$

Thus the ESA gives a measure proportional to the actual laser power spectrum $S_S(\nu)$ translated to low frequencies accessible to electronics. The key to the exceptional sensitivity of the heterodyne method is evident in Equation (2-32) where the detected spectrum strength increases with local oscillator power, P_{LO}. Large local oscillator power translates to better sensitivity.

2.5.2 Delayed Self-Homodyne

On the other hand, the delayed self-homodyne technique (see Fig. 2.9) offers a very simple means to measure the linewidth of an unmodulated laser. This method is wellsuited for linewidth measurements because of the extremely high resolution afforded by using optical interferometers with low-loss fiberoptic delays.

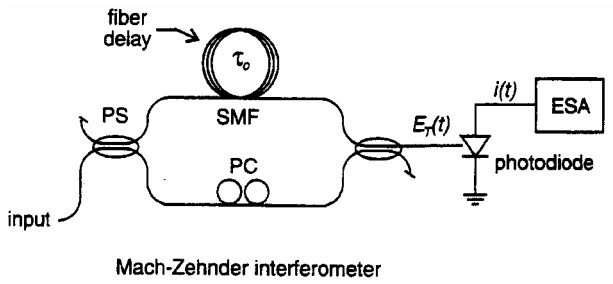

Fig. 2.9 Optical delayed self-homodyne measurement set-up for laser linewidth measurement.

The optical circuit must deliver to the photodetector two fields, one being a delayed replica of the other. The requirement on coherence is satisfied if the differential delay τo of the interferometer satisfies $\tau_0 \geq 1/\Delta\nu$. When this condition is satisfied, the mixing becomes independent of the phases of the interfering light, leading to a more stable measurement.

The photocurrent spectrum for the delayed self-homodyne technique consists of direct detection as well as the desired mixing product but without the frequency shift.

$$S_i(f) \approx R^2\{S_d(f) + 2[S_s(\upsilon) \otimes S_s(-\upsilon)]\}, \quad (2\text{-}33)$$

(ESA =direct detection + self -homodyne spectrum)

where R is the detector responsivity. Since the mixing term is essentially the test-laser spectrum convolved with itself, the displayed lineshape will always be symmetrical, even if the original lineshape had important asymmetries.

The translation of linewidth information from the optical spectrum to the electrical spectrum is illustrated in Figure 2.10. For the case of laser lineshapes described by Lorentzian or Gaussian functions, the displayed electrical power spectrum will have identical functional shapes to the actual optical spectrum. The reason for this is that the shape of these functions are preserved through the autocorrelation operation. The lineshapes of semiconductor lasers are often approximated by a Lorentzian-shaped profile. Note that since the delayed self-homodyne method centers the mixing spectrum at 0 Hz, only half of the

symmetrical spectrum is viewed (see Figure 2.10). Thus the laser FWHM linewidth corresponds to the measured -3 dB frequency point.

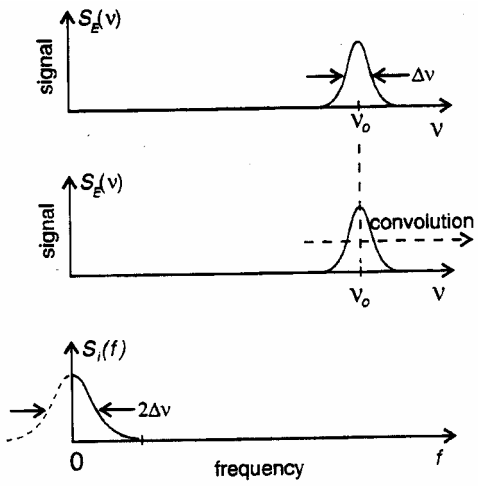

Fig. 2.10 The delayed self-homodyne mixing of the laser filed with itself.

2.6 Results and Discussion

2.6.1. Free-running FPLD and EDFL

In this experiment, the spectra and mode-beating noise characteristics of either EDFL-FPLD or EDFA-FPLD link are compared with those of a commercial DFBLD (Panasonic LNFE03YBE4UP) with linewidth and SMSR of 0.5 MHz and 37.5 dB, respectively, as shown in Fig. 2.11(a) and 2.11(b). Without the mutual injection locked link, the lasing spectrum and the self-heterodyne mode-beating spectrum of a free-running FPLD (at above threshold current of 20 mA) are shown in Fig. 2.11(c) and 2.11(d). The free-running FPLD exhibits a relatively wide lasing spectrum with signal-to-noise ratio (SNR) of about 35 dB. The longitudinal-mode spacing, 3-dB linewidth and SMSR of the free-running FPLD spectrum are 1.2 nm, at least 2 nm and <2 dB, respectively. The linewidth of a single longitudinal mode in the free-running FPLD measured by an OSA is 0.02 nm, which is much broader than that of a DFBLD

with negligible beating noise. On the other hand, the lasing spectrum of a free-running EDFL formed by a close-loop EDFA with 3 dB lasing linewidth and SNR of 1.015 nm and 20 dB is shown in Fig. 2.11(e). A broadened mode-beating noise spectrum has also been observed due to the interference among enormous longitudinal modes in the EDFL cavity, as shown in Fig. 2.11(f). The mode-beating spectrum of EDFL can extend up to several >100 GHz (corresponding to a 3-dB linewidth of 1.015 nm). When an OBPF is added into the EDFL ring cavity, the 3-dB linewidth of the free-running EDFL is further reduced to 0.034 nm, however, the mode-beating noises still exists (with a reduced bandwidth of >4 GHz). Nonetheless, both the free-running and the OBPF filtered EDFLs exhibit large mode-beating noises, which restrict their applications in practical fiber-optic communication networks.

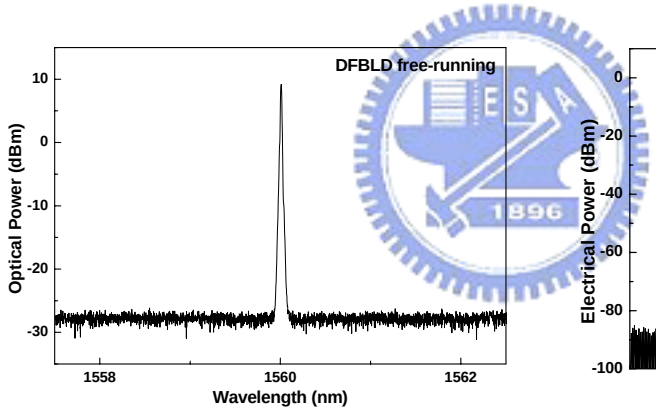

(a)

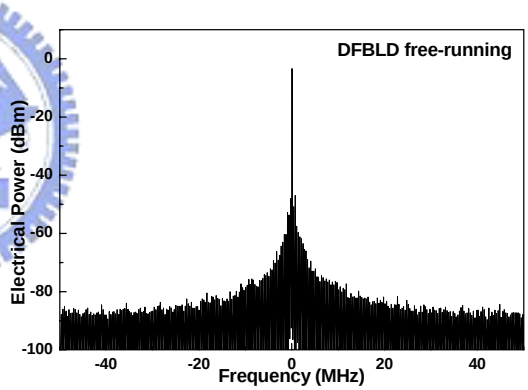

(b)

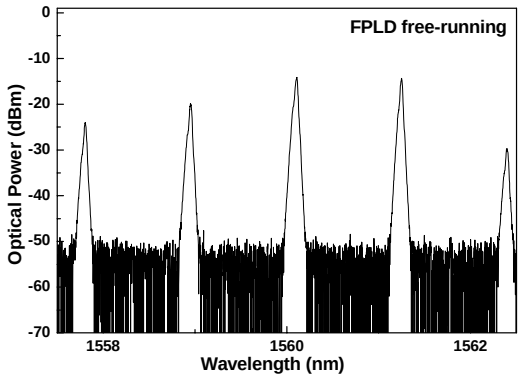

(c)

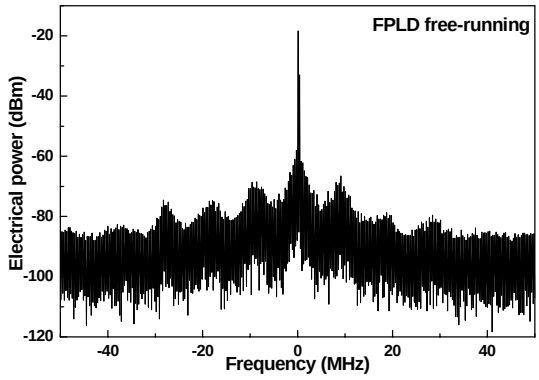

(d)

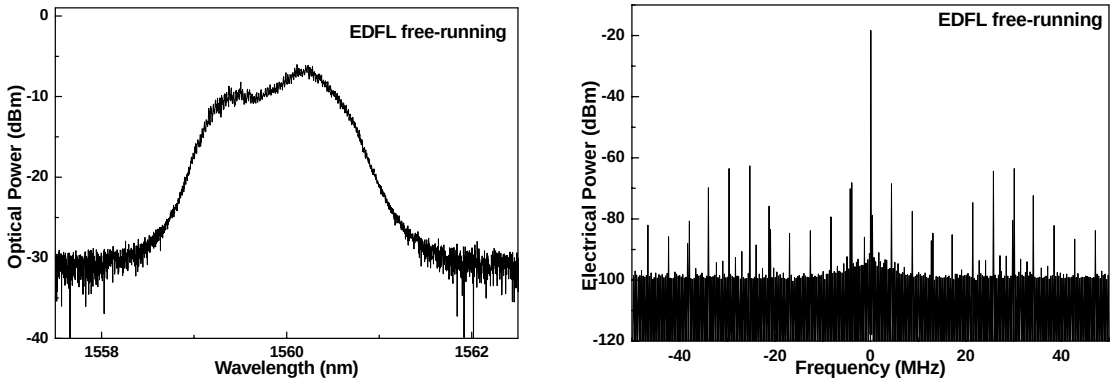

(e) (f)

Fig. 2.11 The lasing and mode-beating spectra of a commercial DFBLD (a) and (b), a CW lasing FPLD (c) and (d), and a free-running EDFL (e) and (f), respectively.

2.6.2. EDFL-FPLD Link with Close-loop EDFA

The lasing spectra of the EDFL-FPLD link driven by different currents (below, near and above threshold current) at 35 ℃ are different, as illustrated in Fig. 2.12. The EDFL-FPLD link exhibits a relatively broadened spectrum when FPLD is biased well below threshold, the lasing linewidth gradually becomes narrow as the mode-selecting capability of the FPLD is initiated at larger biases. One striking feature of the proposed scheme is to operate the EDFL at single FPLD longitudinal-mode regime with high SMSR by driven the feedback-injected FPLD at near-threshold current. It is realized that when the FPLD is operated at nearly lasing regime, the broadband spectrum of the FPLD reveals that there is still a competition among the spontaneously emitted modes. At this stage, even a small intra-cavity feedback power can efficiently lead to single-mode survived in cavity, which eventually suppresses the other lasing modes of the EDFL. The mode-selection is therefore achieved by fine-tuning the power and polarization of the feedback light from the EDFL cavity. The lasing linewidth reaches a minimum when one of the FPLD longitudinal modes is selected by the EDFL-FPLD link due to the combined effects of

gain profile filtering and mutual injection-locking [26]. The SMSR of FPLD can be as high as 48 dB as the partial output of EDFL is filtered and then externally injected back into the FPLD.

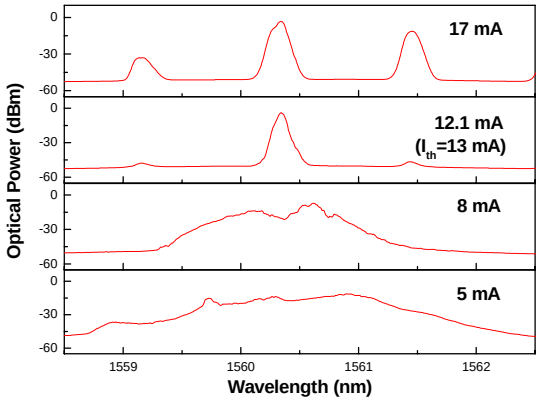

Fig. 2.12 The lasing spectra of an mutually injection-locked EDFL-FPLD link with the FPLD at different biased currents.

According to our simulation, the linewidth of a FPLD longitudinal mode in the EDFL-FPLD link can be further reduced by at least one order of magnitude, however, the SMSR of the EDFL-FPLD link is greatly degraded due to the amplification of the side-modes when FPLD is driven at higher currents above threshold. The mode numbers of the EDFL ring cavity also abruptly increases as the bias current of FPLD arises. The peak wavelength is still dominated by the cross-correlated gain profile of the EDFL and FPLD, while the effect of FPLD is more pronounced. The drift in peak wavelength of the principle lasing mode in the FPLD filtered EDFL under increasing FPLD current is negligible since the EDFL and the FPLD are injection locked each other. Similarly, the beating noise with 4.4-MHz spectral spacing resulting from the EDFL ring cavity cannot be suppressed in such configuration, as shown in Fig. 2.16(b). By measuring the linewidth of such an EDFL-FPLD link in a self-heterodyne optoelectronic interferometric spectrometer (with microwave spectrum analyzer), the exact lasing spectrum of DFBLD and EDFL-FPLD link are compared (see Fig. 2.13).

The measured 3-dB spectral linewidths of DFBLD and EDFL-FPLD link are 3.4 MHz, 19 MHz, respectively. The overall RIN of the DFBLD (thermal and shot noises of the measurement included) rapidly decays to -145 dBm/Hz background at frequency beyond 50 MHz. The RIN of EDFL-FPLD link linearly decreases from -80 dBm/Hz to back-ground within 300 MHz bandwidth.

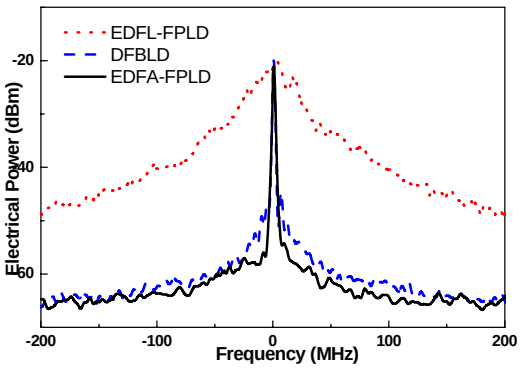

Fig. 2.13 The comparison on the mode-beating spectra of DFBLD, mutually injection-locked EDFL-FPLD link, and EDFA-FPLD link.

2.6.3. EDFA-FPLD Link with Open-loop EDFA

In order to eliminate the side-modes and the mode-beating noise of the EDFL-FPLD link, an EDFA-FPLD link is proposed. The difference between these two configurations is that the EDFA is not constructed in close-loop regime. In this case, there are no resonant cavity modes generating by the EDFA, which only amplifies the spontaneous emission from FPLD and feedback seeds into the FPLD after filtering. A best SMSR can be obtained by setting the FPLD at 35^{o}C and just-below-threshold driving condition and selecting the appropriate coupler ratio (OC1) of the EDFA-FPLD link. Fig. 2.14 shows the optical spectra of EDFA-FPLD link with different coupling ratios of OC1. When FPLD is injected by the filtered ASE from EDFA with power of 0.37 mW (using OC1 with coupling ratio of 5%), it is seen that the other longitudinal modes of FPLD are growing up to be competitive the

principle mode. This eventually leads to a bad SMSR of only 23 dB, as shown in Fig. 2.14(a).

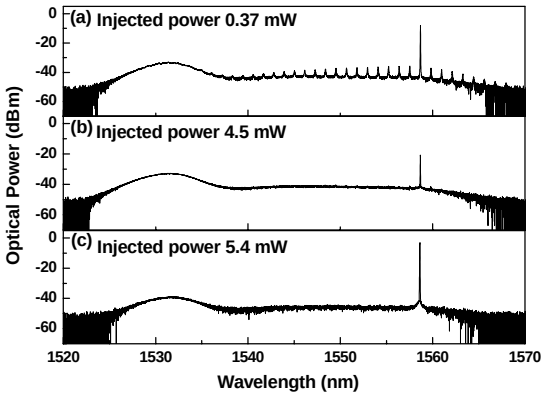

Fig. 2.14 The optical spectra of mutually injection-locked EDFA-FPLD link with different coupling schemes (a) 5% EDFA feedback injects into the FPLD (b) 95% EDFA feedback injects into the FPLD (c) 50% EDFA feedback injects into the FPLD.

To improve, the coupling ratio of OC1 and the mutual injecting power for the FPLD in Fig. 2.1(c) is adjusted. Although there is only the dominant mode lasing under the strong mutual injection, the SMSR is still 25 dB as the feedback injecting power increases to 4.5 mW (using OC1 with coupling ratio of 95%), as shown in Fig. 2.14(b). The highest SMSR of 42 dB (see Fig. 2.14(c)) is obtained with a mutual injection power of 5.4 mW (using a 50% coupling ratio in this scheme), where the corresponding 3-dB linewidth of the EDFA-FPLD link is reduced to 0.016 nm. Note that the minimum linewidth of the mutually injection-locked EDFA-FPLD link ever obtained is as small as 0.012 nm, which is achieved by high-power seeding the unbiased FPLD at a cost of worse SMSR. The 3-dB spectral linewidth of EDFA-FPLD link measured by interferometeric method is comparable with that of a DFBLD (see Fig. 2.13). In comparison with the EDFL-FPLD link, the EDFA-FPLD link not only suppresses beating noise but also reduces the 3-dB linewidth by almost one order of magnitude. In fact, the feedback injection from the filtered EDFA is equivalent to an increase on the end-face reflectivity of FPLD, which inevitably leads

to the reduction of linewidth and the improvement of SMSR in mutually injection-locked EDFA-FPLD link. These results have also been confirmed by our simulation, as shown in Fig. 2.3 and 2.5. To compare, the lasing spectra of the free-running EDFL, the OBPF filtered EDFL, the EDFL-FPLD link, and EDFA-FPLD link are illustrated in Fig. 2.15.

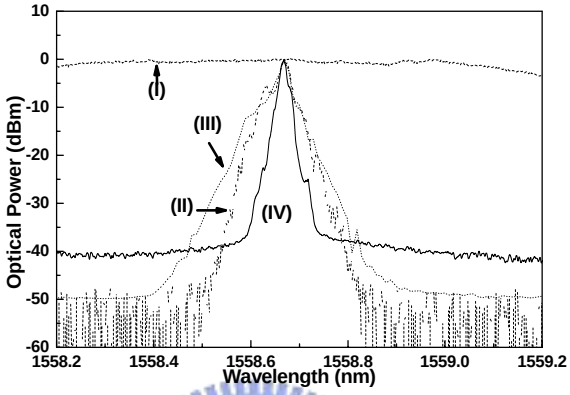

Fig. 2.15 The lasing spectra of (I) free-running EDFL, (II) OBPF filtered EDFL, (III) mutually injection-locked EDFL-FPLD link, and (IV) mutually injection-locked EDFA-FPLD link.

Obviously, the free-running EDFL exhibits a relatively wide-band lasing spectrum. The 3-dB linewidth of the OBPF filtered EDFL is reduced to 0.034 nm. The OBPF filtered EDFA-FPLD link can further reduce the linewidth to 0.012 nm, which is even better than that of EDFL-FPLD link. Furthermore, the measured spectral linewidths of the OPBF filtered EDFA-FPLD link and EDFL-FPLD link are 0.03 nm and 0.05 nm at 10-dB decay, respectively. The characteristic parameters of the aforementioned systems are listed on Table 2.1.

Table 2.1 The 3-dB linewidths (Δλ), SMSR, and required injecting power for the FPLD at different laser configurations.

Configurations	Injection (mW)	Linewidth (MHz)	SMSR (dB)
EDFL Free-running		1.27×10^5 (or 1.015 nm)	36
OBPF filtered EDFL		4.25×10^3 (or 0.034 nm)	45
DFBLD		3.4	~40
EDFL-FPLD Link	8.63	19	48
EDFA-FPLD Link	0.37	3.4	23
EDFA-FPLD Link	4.5	3.4	25
EDFA-FPLD Link	5.4	3.4	42

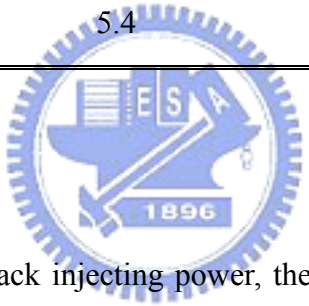

2.6.4. Discussion

Even at a higher feedback injecting power, the EDFL-FPLD link still exhibits a larger linewidth, which is attributed to the interference of enormous longitudinal modes in the EDFL cavity with free spectral range of about 4.4 MHz. Without these modes, the EDFA-FPLD link can reach a smaller linewidth and nearly mode-beating-noise free lasing spectrum at low-feedback injecting condition. Although the best SMSR of up to 48 dB can be obtained from the mutually injection-locked EDFL-FPLD link, the side-modes are still observable in the lasing spectrum, as shown in Fig. 2.16(a). Such a configuration inevitably increases the mode-beating noises (see Fig. 2.16(b)). In contrast, the side-modes are completely eliminated in the mutually injection-locked EDFA-FPLD link (see Fig. 2.16(c)), and a nearly clean mode-beating spectrum can be observed in Fig. 2.16(d). The adding of

intra-cavity OBPF in the EDFA-FPLD helps the elimination of FPLD side-modes, while the use of open-loop EDFA avoids the EDFL longitudinal modes.

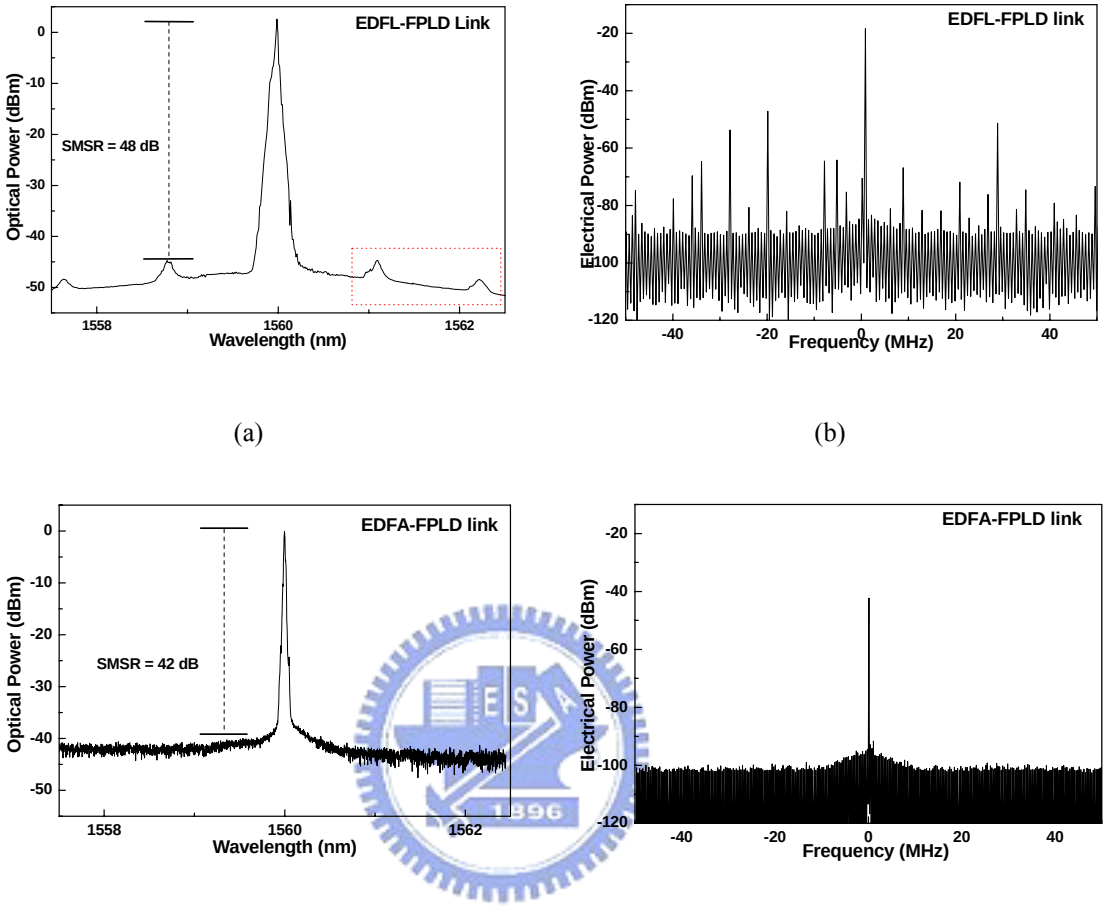

Fig. 2.16 The lasing and mode-beating spectra of EDFL-FPLD (a) and (b), and EDFA-FPLD links (c) and (d).

In addition, the FPLD is operated at just below threshold current in our experiment, corresponding to an output power of below 0.1 mW. Although the EDFA can provide very large gain for such a small input signal (see Fig. 2.17), the maximum output power of the EFDA-FPLD link is still limited at 20 mW. Since the insertion loss of the 50% output coupler added into the EDFA-FPLD link is about 3.3 dB, and the output of the EDFA-FPLD link is further attenuated by 10 dB (coupling ratio of 10%, as shown Fig. 2.1). In comparison, the maximum output power of a commercial DFB laser diode can be 10-40 mW. To enlarge the output power of the

EDFA-FPLD link, the use of an FPLD with larger output power is mandatory. With these ameliorations, a DFBLD-like performance of the EDFA-FPLD link can be obtained. This design has already improved the overall performances of previous demonstration (the EDFL-FPLD link), which also corroborates the niche of amplified feedback seeding in mutual injection-locking laser system for linewidth reduction and SMSR enhancement. The use of FPLD in the EDFA for ultra-narrow band-pass filtering and beating-noise suppression is thus straightforward.

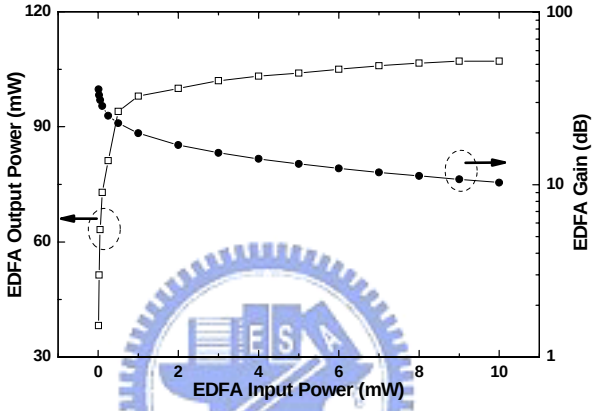

Fig. 2.17 The output power and gain characteristics of EDFA at different input powers.

2.7 Conclusion

In conclusion, we theoretically analyze the effect of feedback seeding power for FPLD on the linewidth, SMSR, and mode-beating noise characteristics of a mutually injection-locked EDFL-FPLD or EDFA-FPLD link. The SMSR and 3-dB linewidth of such link as a function of feedback power dependent reflectivity change are simulated. By comparing the EDFL-FPLD link with the EDFA-FPLD link, it is fount that the side-mode in the EDFA-FPLD link can be entirely suppressed due to the effects of mutual injection-locking, intra-cavity OBPF and active FPLD filtering. To help selecting the strongest mode from the gain-spectrum of FPLD lasing in the

EDFA-FPLD link, the FPLD must be biased at just below threshold condition. The narrowest 3-dB linewidth of 3.4 MHz and comparable SMSR of 42 dB in an EDFA-FPLD link are obtained under a feedback injecting power of 5.4 mW. Furthermore, the EDFA-FPLD link exhibits a better beating noise suppression performance as compared to the EDFL-FPLD link. The maximum output power of the current EFDA-FPLD link is limited at 20 mW, and the improvement relies on the use of an FPLD with larger output power. With the improved mutual injection-locking scheme, a mode-beating-noise free, single-mode and high-SMSR EDFA-FPLD link is primarily demonstrated, which has a comparable performance with commercial DFBLD sources.

Chapter 3

All-optical NRZ-to-PRZ format transformer by injection-locking an Fabry-Perot laser diode at unlasing condition

3.1 Abstract

The all optical format conversion of nonreturn-to-zero- (NRZ-) into a pseudo-return-to-zero- (PRZ-) data-stream is demonstrated by using a synchronously modulated Fabry-Perot laser diode (FPLD) at below threshold condition. The NRZ-to-PRZ transformation is implemented by externally seeding and gain-switching the FPLD with an optical NRZ data stream. The optimized RF driving power of the FPLD is ranged between 24.4 dBm and 24.7 dBm. The on/off extinction ratio (ER) and side mode suppression ratio (SMSR) of the FPLD based data transformer are severely dependent on external injecting wavelength and power. At optimized injecting level of -2 dBm, the maximum ER and SMSR of the injection-locked FPLD up to 12.2 dB and 40 dB are obtained when the injecting wavelength is coincident well with the FPLD longitudinal mode. Linewidth broadening of injection-locked FPLD from 0.04 to 0.19 nm at 10-dB decay is also observed at mode matching condition. The smallest timing jitter and narrowest pulsewidth of gain-switched PRZ pulses from FPLD are 0.4 ps and 44 ps, respectively. With the received optical power and external injection power of larger than -22 dBm and 6 dBm, respectively, the BER of PRZ data-stream at 2.488 Gbit/s can be smaller than 10^{-12}. The power penalty of the FPLD based NRZ-to-PRZ data transformer can be smaller than 1.2 dB at a BER of 10^{-9}.

The maximum NRZ-to-PRZ conversion rate of the FPLD can be up to 9.953 Gbit/s by increasing DC-biased current of the FPLD with a power penalty of 1.5 dB at a BER of 10^{-9}. In application, an all-optical OR gate is realized by using the FPLD-based NRZ-to-PRZ format transformer with a 3-dB coupler.

3.2 Introduction

Recently, the Fabry-Perot laser diode (FPLD) based ultrafast all-optical signal processing systems are expected to play major roles in future all-optical networks (AONs) [11-16]. Versatile all-optical controlled signal processing techniques such as the clock frequency division [11,12], the wavelength conversion [13], the upstream traffic transmission [14], and nonreturn-to-zero- (NRZ-) to-pseudo-return-to-zero (PRZ) format transformation [15,16], have been demonstrated. To date, there are several methods reported to implement NRZ-to-PRZ transformation in FPLDs. Chow *et al.* proposed an all-optical NRZ-to-PRZ format transformer structure, which is achieved by injection-locking a CW-lasing FPLD with a gain-switched pulse at one longitudinal mode of the FPLD, and concurrently seeding the FPLD with a optical pseudo-random binary sequence (PRBS) encoded data-stream at the another longitudinal mode of the FPLD [15]. Hence, simultaneous wavelength-conversion and NRZ-to-PRZ format conversion can be achieved with a negative power penalty of -9.5 dB at a bit-error-rate (BER) of 10^{-9}. In addition, such a module was proposed to operate over a 45-nm wavelength range with an extinction ratio (ER) exceeding 10 dB. Alternatively, Jeong *et al.* employed transverse-magnetic (TM) mode absorption and the self-phase modulation (SPM) characteristics of an FPLD to achieve the function of NRZ-to-PRZ data format conversion [16]. The FPLD exhibits absorption nulls for TM-mode injection which carried an NRZ data-stream and experiences the SPM induced blue/red

frequency chirp at rising/falling edge. By extracting the chirp components, all-optical NRZ-to-PRZ format converted data-stream can be obtained. In viewing of these results, the use of FPLD in all-optical data format transformation system has become a promising topics in studying the high-speed AONs, and the gain-switching of FPLD has been shown as the simplest way to produce PRZ data-stream at arbitrary data rates. However, such a cheap device exhibits drawbacks of multimode lasing spectrum [29], low side-mode suppression ratio (SMSR) and ER that degrade the performances of PRZ data transmission and decoding. To overcome, various approaches enabling single-mode and wavelength-tunable FPLD operations via self-seeding and external-injection seeding schemes were emerged [30-32]. The self-seeding feedback technique selects a specific wavelength component from the FPLD output, which results in a single-mode optical pulse emission within the pulse build-up time of the FPLD. Wavelength tuning can also be achieved by using the wavelength-selective element, which although changes the repetition frequency or the cavity length equivalently. In configuration with fiber Bragg gratings, such an self-seeded FPLD has recently developed as a low-cost alternative to the commonly used continuous-wave tunable lasers source [33]. However, the side mode suppression ratio (SMSR) of previous implementations are still low (<20 dB) and the wavelength tuning ranges are relatively small (about 10 nm). In contrast, the repetition frequency and the external cavity length can remain as constant in a CW external-injection scheme. In this case, the FPLD gain-switched by external injection of a tunable laser source can be single-mode lasing when the injected wavelength coincides with the longitudinal mode of the FPLD. More recently, mutual injection locking of two gain-switched FPLD [34, 35] has been employed to convert multi-mode into a stable single-mode lasing via the use of dispersion compensating fiber and the control of

delay-time between the radio-frequency (RF) signals driving the lasers.

By taking the advantages of gain-switching and external injection-locking techniques, we propose a new NRZ-to-PRZ data conversion scheme by injecting a single-mode optical NRZ data into a synchronously modulated FPLD at unlasing condition. Unlike the previously reported methods, no additional DFBLD is required to achieve NRZ-to-PRZ operation in our case. Therefore, a lower-cost and simpler NRZ-to-PRZ transformer can be achieved. In contrast to previous approaches, the FPLD is operated without DC driving current, and is synchronously modulated by the RF clock signal with its maximum current equivalent to the threshold of the FPLD. The FPLD is neither lasing nor gain-switching in this case. When the FPLD is injected by an incoming optical NRZ data with high level ("1" bit), the threshold current of the FPLD is reduced and the gain-switching as well as the PRZ data-stream is generated from the FPLD. Such an external injection not only achieves the NRZ-to-PRZ transformation, but also helps to suppress the spontaneous emission and the gain of side modes. This eventually enhances the SMSR and reduces the noise level of the FPLD based data format transformer. Furthermore, with this configuration, the highest data rate of 9.953 Gbit/s can be achieved by slightly raising the DC bias of the FPLD (below the threshold condition). In Section 3.3, the experimental setup and operating principle are described. In Section 3.4, the experimental results and related discussion are presented. In Section 3.5, the all-optical logical OR-gate operation is demonstrated. Finally, the conclusions are summarized in Section 3.6.

3.3 Experimental Setup and Principle of Operation

The setup of a FPLD-based NRZ-to-PRZ transformer is shown in Fig. 3.1.

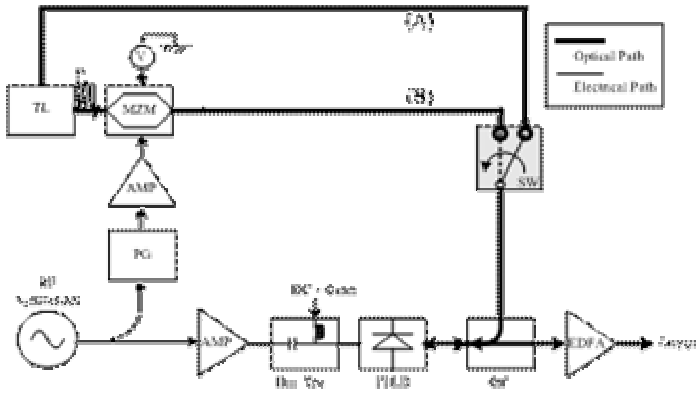

Fig. 3.1 Experimental setup for the NRZ-to-PRZ format transformer: AMP: power amplifier; EDFA: Erbium-doped fiber amplifier; FPLD: Fabry-Perot laser diode; MZM: Mach-Zehnder modulator; OC: optical coupler; PG: pattern generator; SW: optical switch; TL: tunable laser, PC: polarization controller.

The FPLD with threshold current and longitudinal mode spacing of 13 mA and 1.2 nm is synchronously modulated by the amplified RF clock signal. The modulating power of FPLD is adjusted at just below threshold condition (24.4 dBm). At low bit-rate transmission condition, the FPLD is only driven by the amplified RF signal via a Bias Tee circuit without any DC driving current. The temperature of FPLD is controlled at 27.5^{o}C with fluctuation of <0.1 ^{o}C to prevent the drift in the wavelength of the FPLD's longitudinal modes. In first experiment, the optimized condition for external-injection-induced gain-switching of FPLD is investigated. (see optical path (A) in Fig. 3.1). One branch of a 3dB optical coupler (OC) is employed to connect a tunable laser (TL, Hewlett Packard, 8168F), which externally injects continuous-wave (CW) light into the FPLD, and the other branch transmits the gain-switched FPLD into an EDFA for pulse amplification. To simulate an incoming optical data stream with NRZ format in second experiment, a amplified PRBS pattern generated from Pattern Generator (Hewlett Packard, 70843B) is used to drive the Mach-Zehnder intensity modulator (MZM, JDS Uniphase, OC-192 Modulator), which then encodes the TL at wavelength matching the specific longitudinal mode of the FPLD (see optical path (B) in Fig. 3.1). A transfer function of the MZM with Vπ of 5 V is shown in Fig. 3.2.

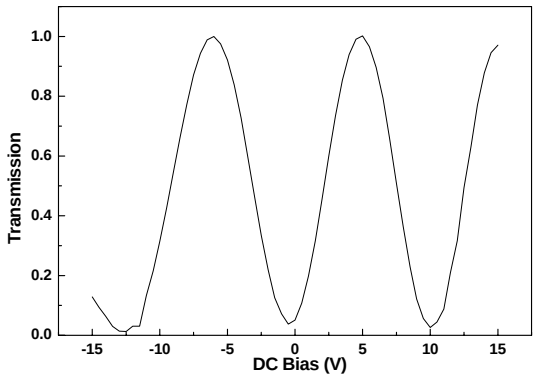

Fig. 3.2 The characteristic transmission coefficient of MZM at different DC bias.

The MZM is biased at 7.5 V (nearly at the linear operating region), and is encoded by a PRBS pattern with amplitude of 5 V. This results in a PRBS-encoded optical NRZ signal with largest on/off ER. 10% of the EDFA is coupled out to monitor the optical spectrum and the pulse waveform via an optical spectrum analyzer (OSA, Ando, AQ6317B) and a digital sampling oscilloscope (DSO, Agilent, 86100A with 86106A module), respectively. Finally, the BER of the NRZ-to-PRZ signal optoelectronic converted by a clock/data receiver (Agilent, 83493A) is measured by using an error detector (Hewlett Packard, 70843A).

Figure 3.3 illustrates the operating principle of 'general' gain-switching and non-dc-biased gain-switching methods. In Fig. 3.3(a), the DC bias current is set at near threshold and a large sinusoidal signal with power of greater than 27 dBm is applied to gain-switch the FPLD. In Fig. 3.3(b), the DC bias current is set at 0 mA and the sinusoidal signal is applied to approach the threshold of the FPLD (see the line (A) in Fig. 3.3(b)). Under such a setting condition, the FPLD is originally unlasing.

The principle of NRZ-to-PRZ transformation is described below. First, the derived threshold current can be expressed as

$$I_{th} = \frac{e}{g\tau\tau_p} \tag{3-1}$$

where e is the electron charge g is the stimulated recombination coefficient, τ is the

electron lifetime, and τ_p is the photon lifetime [36].

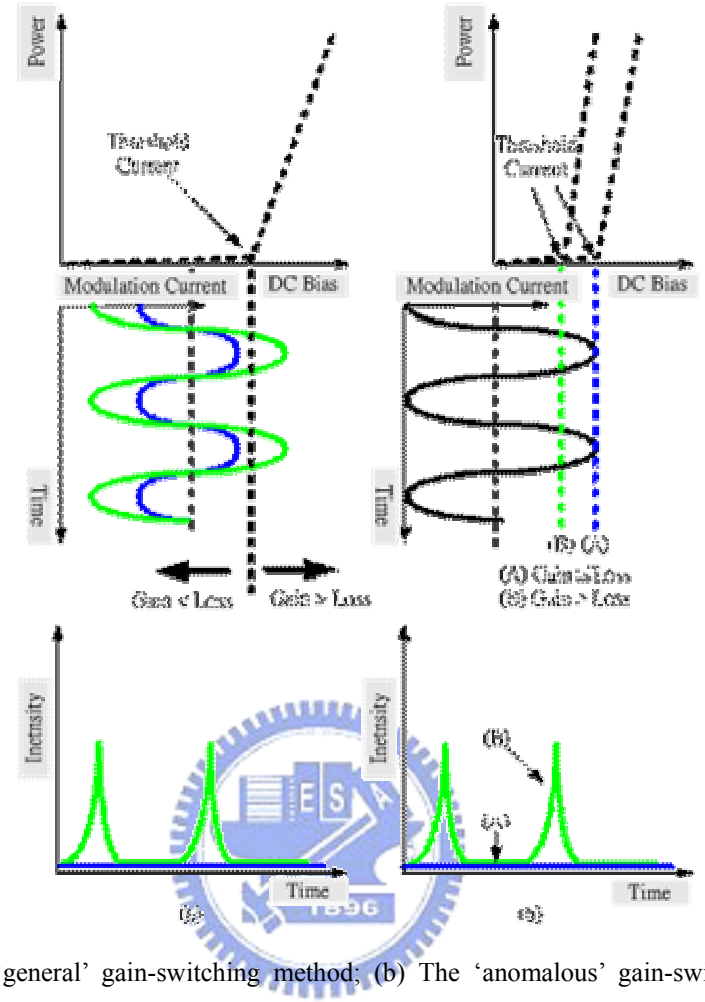

Fig. 3.3 (a) The 'general' gain-switching method; (b) The 'anomalous' gain-switching method: (A) without external injection; (B) with external injection.

In particular, the stimulated recombination coefficient g can also be written as a function of external injection power, that is

$$g = g_e + \frac{\eta P_{ext}}{h\nu} \tag{3-2}$$

where g_e is the original value under the electrically-driving case, P_{ext} is the power by external injection light, η is the quantum efficiency of optoelectronic conversion, h is the Planck constant, and ν is the carrier frequency. The eqn. (3-1) can be re-written as

$$I_{th} = \frac{e}{\left(g_e + \frac{\eta P_{ext}}{h\nu}\right)\tau\tau_p} \tag{3-3}$$

As a single-mode CW light externally injects into the FPLD, the effective stimulated recombination coefficient g is increased (due to the increase of P_{ext}) and thus the threshold current of the FPLD is decreased (see the line (B) in Fig. 3.3(b)). Under the external injection, the unlased FPLD turns to be gain-switching due to the reduction of the effective threshold current. Based on such an anomalous operation, the FPLD can thus be employed to convert the externally seeded optical NRZ data-stream into a PRZ one. The high level ("1" bit) data will cause the FPLD gain-switching, whereas low level ("0" bit) data remains the FPLD unlasing. As a result, an NRZ-to-PRZ data format transformation can be achieved.

Moreover, when the laser diode produces the gain-switched pulses, the corresponding linewidth on the optical spectrum becomes broadened. The laser wavelength is strongly related to the time dependency of the carrier concentration, since the effect of free carriers on the refractive index of the semiconductor material is involved. The instantaneous wavelength is related to the refractive index as

$$\lambda(t) = \frac{n(t)}{n_0}\lambda_0, \tag{3-4}$$

where $n(t)$ and n_0 are the time-dependent and original refractive indices, respectively. In general, the free carrier plasma refraction, the band-gap shrinkage, and the dynamic Burstein-Moss shift are the principal mechanisms by which the carrier concentration affects the refractive index [37]. Even though, the carrier-induced refractive index changes still depend upon a number of factors, and the exact expression of n as function of carrier density is complicated. For simplicity, we can write

$$n(t) \cong \frac{dn}{dN}N(t), \tag{3-5}$$

where $N(t)$ is the time-dependent carrier density in FPLD. Combining the eqn. (3-4) and (3-5), the linewidth broadening of FPLD under the gain-switched condition can be obtained, that is,

$$\Delta\lambda \cong \frac{\lambda_0}{n_0}\frac{dn}{dN}\Delta N\,, \qquad (3\text{-}6)$$

3.4 Results and Discussion

3.4.1 CW external injection

The FPLD is synchronously modulated by RF clock signal with power and repetition frequency of 24.4 dBm and 1 GHz, respectively, which makes the FPLD below its lasing threshold. With an external optical injection power of -2 dBm at central wavelength coincident with the FPLD's longitudinal mode, the effective threshold current of the FPLD is reduced and the FPLD can be gain-switching. The pulsewidth and peak power of the gain-switched FPLD after EDFA amplification are 44 ps and up to 135 mW (corresponding to average power of 22 mW). Later on, the wavelength of the TL is detuned away from the longitudinal mode of the FPLD to evaluate the wavelength detuning range of the external injection-locked FPLD. The wavelength detuning causes the gain-switching pulses to degrade and diminish when $\Delta\lambda \geq 0.4$nm, as shown in Fig. 3.4.

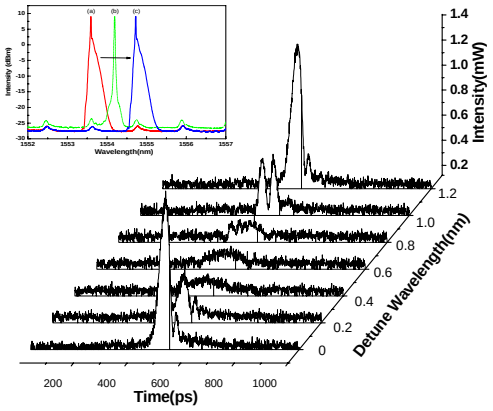

Fig. 3.4 The evolution of pulse-shape under the external injection at different wavelengths.

As the injection wavelength completely coincides with one of the FPLD mode,

the maximum SMSR of 34 dB can be obtained, which is better than the FPLD operated at wavelength mismatching condition, as shown in the inset of Fig. 3.4. The wavelength matching between the external injection laser and the longitudinal mode of FPLD is mandatory for generating gain-switched pulses with largest peak power and highest SMSR.

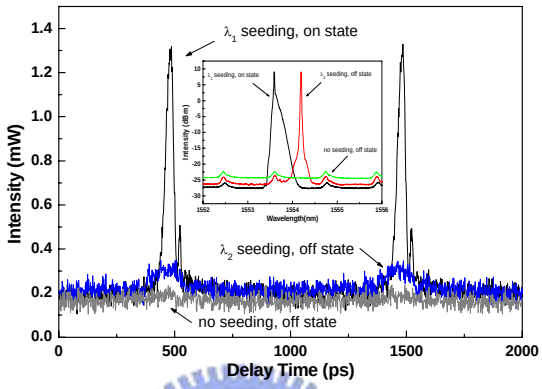

Fig. 3.5 The OOK pulse shape of the injection-locked FPLD at "on" and "off" states with repetition rate of 1 GHz.

Under the precise control of external injection wavelength, the on/off extinction ratio (ER) of the gain-switched FPLD pulse-train (defined as the amplitude ratio of wavelength-matched to wavelength-mismatched pulse) can be optimized. By changing the external injection wavelength between λ and λ+0.6 nm, the maximum ER of FPLD pulse-train under wavelength controlled OOK procedure is about 10.5 dB (see Fig. 3.5). Similarly, the ER of FPLD pulse-train can be also defined as the amplitude ratio of with to without external injection. The ER of the injection-locked FPLD pulse-train is up to 12.2 dB under the on/off control of external injection power (see Fig. 3.5). The amplified spontaneous emission (ASE) of the FPLD is slightly higher without the injection of the TL, as shown in the inset of Fig. 3.5. This indicates that the suppression of the ASE and side modes of the FPLD under external injection from the TL is more pronounced than those of the FPLD at normal operation.

This is mainly attributed to the reduction of effective threshold current of the FPLD under the external injection case. In addition, a relatively weak signal with considerable noise has also been found as the injection wavelength is detuned away from the FPLD's longitudinal mode by 0.4 nm.

The lasing spectra of the CW free-running FPLD, the CW tunable laser, and the gain-switched FPLD are illustrated in Fig. 3.6. The measured spectral linewidth for one longitudinal mode of the CW free-running FPLD are 0.015 nm and 0.04 nm at 3- and 10-dB decay, respectively. When the FPLD is gain-switching, the 10-dB linewidth significantly broaden to 0.19 nm. This result correlates well with the theory that the transient variation in carrier density simultaneously affects the refractive index and mode linewidth of the gain-switched FPLD.

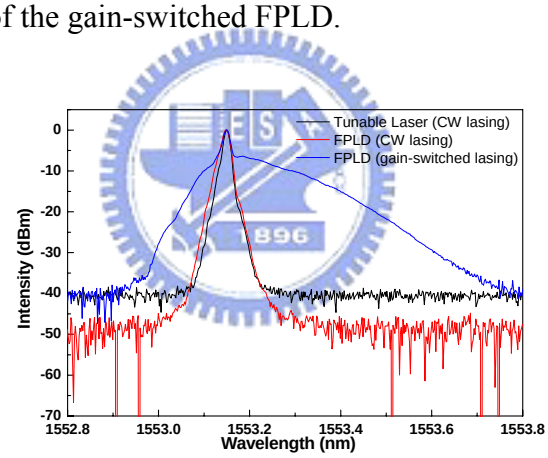

Fig. 3.6 The linewidth comparison of the CW free-running FPLD, the CW tunable laser, and the gain-switched FPLD

Moreover, the variation in RF driving power and external injection power can strongly affect the on/off ER (with and without external injection) of the gain-switched FPLD operated at injection-locking mode (see Fig. 3.7). When RF driving power is below 24 dBm, the ER is extremely small (see trace (a) in Fig. 3.7). It is found that the tolerance on RF driving power for optimized ER of FPLD pulae-train is relatively severe, only 1 dB increasing of RF power will cause a serious degradation on the ER

of FPLD pulse-train. The optimized RF driving power is ranged from 24.4 to 24.7 dBm. In particular, when RF driving power is set at just below threshold, there is a trade-off between the ER of FPLD pulse-train and the external injection power. Larger external injection power contributes more to the CW component of FPLD and thus degrades the ER.

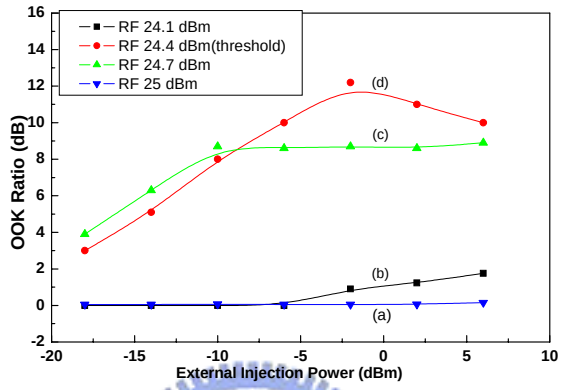

Fig. 3.7 The extinction ratio of the injection-locked FPLD at different RF and external injection power.

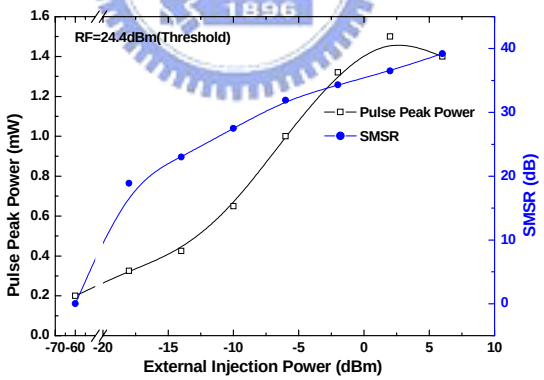

Fig. 3.8 The peak power and the SMSR of the single-mode gain-switched FPLD at OOK mode.

The peak power and SMSR of the single-mode gain-switched FPLD at different injection powers are shown in Fig. 3.8. The best SMSR of 40 dB under injection power of 6 dBm is obtained at a cost of slightly decreasing peak power (~140mW). At wavelength-matched condition, the lowest noise performance is obtained from the injection-locked FPLD. The single-side-band (SSB) phase noise and the associated

timing jitter of the gain-switched pulses are also evaluated. With external injection power of 6 dBm, the gain-switched FPLD pulses exhibit SSB phase noise as low as -100 dBc/Hz at 5 kHz offset from carrier frequency (see Fig. 3.9). The corresponding rms timing jitter of 0.4 ps calculated over an integral frequency band between 10 Hz and 5 kHz is also shown in Fig. 3.9.

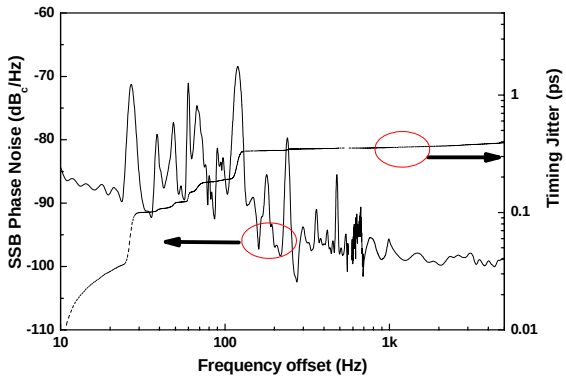

Fig. 3.9 The SSB phase noise density and associated timing jitter of the injection-locked FPLD pulses.

Furthermore, the rms timing jitter of the gain-switched pulse as a function of external injection power is also depicted in Fig. 3.10. The timing jitter of the injection-locked and gain-switched FPLD decreases from 0.7 ps to 0.4 ps as the external injection power increases from -14 dBm to 6 dBm. In principle, the rms timing jitter is proportional to the ratio of the standard deviation to the mean value of the cavity photon density around time t_o, where t_o is the time corresponding to the threshold carrier density reaches the threshold. On condition that the injection power is smaller, the timing jitter is dominated by spontaneous emission of the FPLD. As the injection power is increased, the externally injected light provides a stimulated emission which is well above the level of spontaneous emission in the FPLD cavity. The stimulated emission reduces relative fluctuations in the photon density around t_o, which leads to a significant reduction in rms timing jitter [38]. As a result, the pulsewidth of gain-switched FPLD slightly shortens from 47 ps to 44 ps with the

increase of the external injection power.

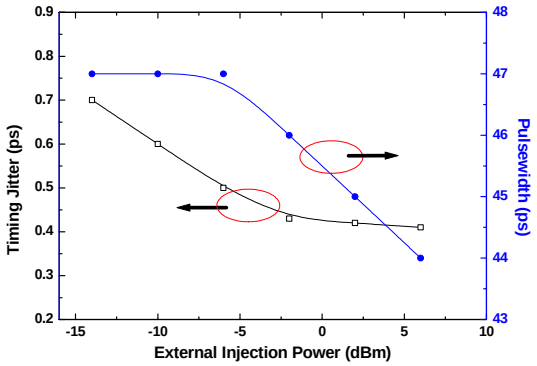

Fig. 3.10 Timing jitter and pulsewidth versus external injection power.

3.4.2 External injection by PRBS coding

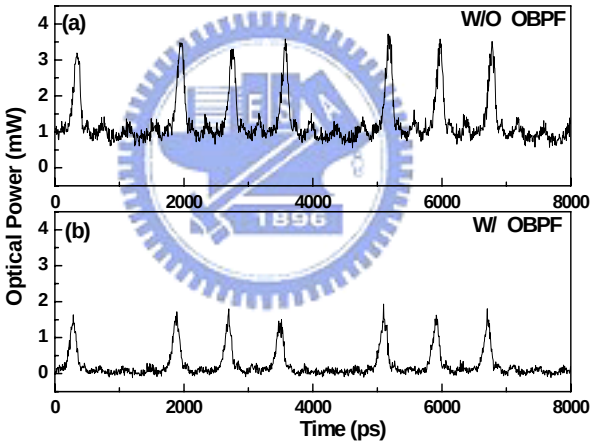

Fig. 3.11 RZ data stream (a) without OBPF (b) with OBPF.

In this experiment, an incoming optical NRZ data-stream generated by encoding the external injection laser with a PRBS-signal drived MZM is employed to seed the synchronously modulated FPLD at below threshold condition. The FPLD receives the incoming NRZ data-stream and initiates the all-optical NRZ-to-PRZ transformation procedure. A clean PRZ data stream can be obtained after passing the FPLD output through optical band-pass filter (OBPF), as shown in Fig. 3.11. Without the OBPF,

the PRZ data-stream carries a large ASE from the EDFA, giving rise to an increased CW component and a worse quality in the communication data. The adding of OBPF completely eliminates the 1-mW CW component and results in a clean PRZ data stream with the optimum eye diagram.

(A) The NRZ-to-PRZ performance at 2.488 Gbit/s (sonet SDH, OC-48)

Figure 3.12 shows the example for the electrical NRZ data-stream before the MZM, the optical NRZ data-stream on the external injection carrier, and the transformed PRZ data-stream generated from the injection-locked FPLD at a sonet-SDH data rate of 2.488 Gbit/s, respectively. For example, an 8-bit edited NRZ pattern 01011101 (Fig. 3.12(a)) is sent into the MZM, and the logically inverted optical NRZ pattern 10100010 is obtained at the MZM output port (Fig. 3.12(b)). After injecting into the FPLD, the NRZ data-stream is transformed to PRZ-format with identical pattern of 10100010, as shown in Fig. 3.12(c). Such a PRZ-format data can also be the potential candidate of carrier in a time-division multiplexing (TDM) system, which essentially helps to improve the bit rate and increase the network throughput.

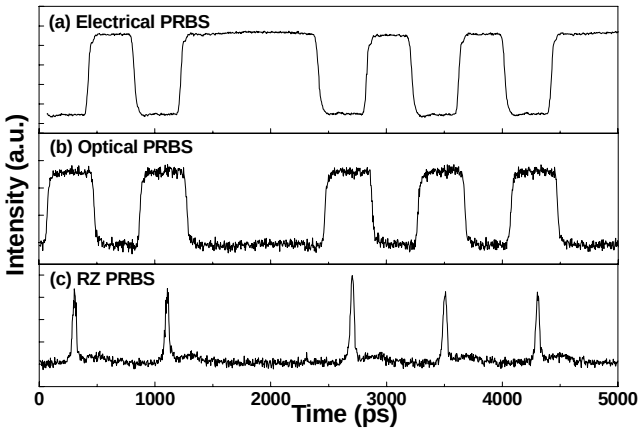

Fig. 3.12 The patterns: (a) the electrical NRZ data before the MZM; (b) the PG-encoded external injection light; (c) the transformed PRZ signal generated from the injection-locked FPLD.

The data rate is 2.488 Gbit/s.

The eye diagrams of the electrical NRZ data-stream before the MZM, the optical NRZ data-stream after MZM, and the transformed PRZ data-stream generated from the injection-locked and gain-switched FPLD, respectively, as shown in Fig. 3.13. A clear and open eye is still observable for the PRZ-format data-stream, although it carries larger amplitude noise than that of the optical NRZ data due to the existence of the considerable spontaneous emission noise at the non-injected condition (*i.e.* "0" state).

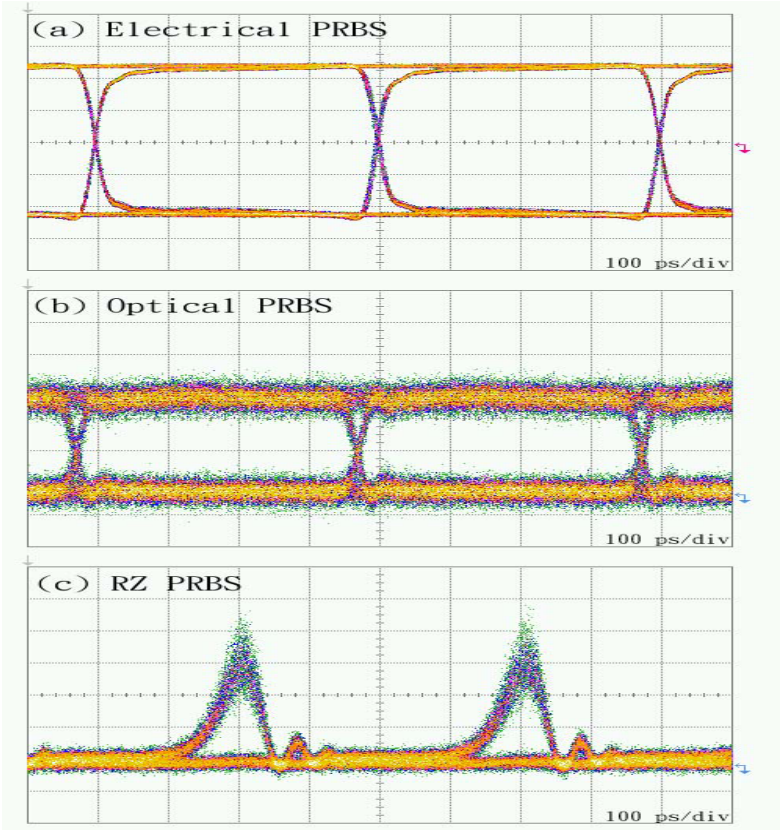

Fig. 3.13 The corresponding eye diagrams: (a) the electrical NRZ data before the MZM; (b) the PG-encoded external injection light; (c) the transformed PRZ signal generated from the single-mode FPLD. The data rate is 2.488 Gbit/s

With a input of 2^{23}-1 bit PRBS NRZ data-stream at 2.488 Gbit/s, the BER of the NRZ-format optical data and the transformed PRZ-format data at different receiving powers are depicted in Fig. 3.14. The NRZ-to-PRZ data transformer has power

penalty of less than 1.2 dB at a BER of 10^{-9}. Such a power penalty mainly results from the spontaneous emission noise of FPLD at bit 0 and the considerable amplitude fluctuation at bit 1. And error-free (BER < 10^{-12}) PRZ-format data can be received at optical power of -22 dBm at least.

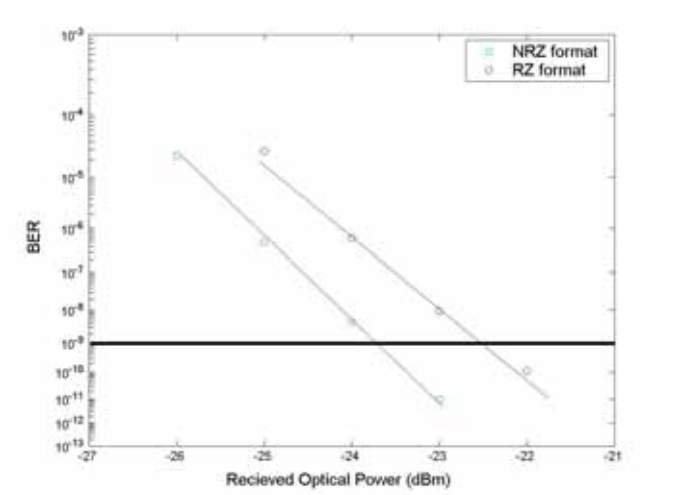

Fig. 3.14 The BER against the received optical power for NRZ-encoded external injection light and transformed PRZ signal at data rate of 2.488 Gbit/s

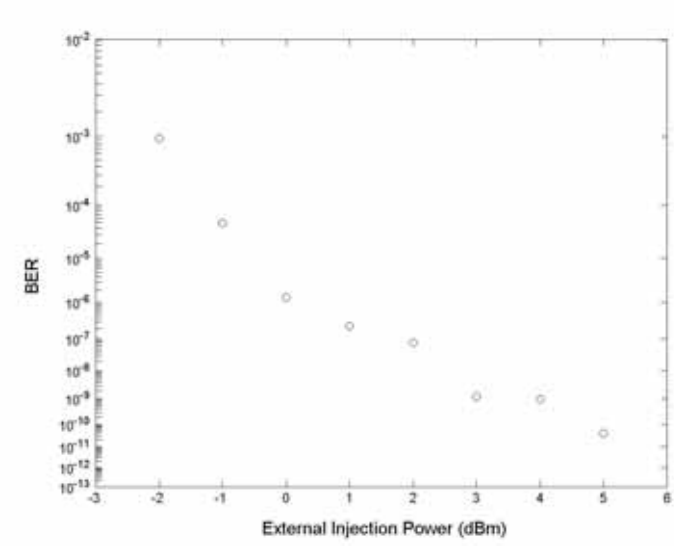

Fig. 3.15 The BERs for different external injection powers at data rate of 2.488 Gbit/s.

The BER of PRZ-format data is also affected by the external injection power, as shown in Fig. 3.15. When external injection power is larger than 3 dBm, the BER of the received PRZ-format data can be as small as 10^{-9}. Moreover, the error-free result

can be observed under external injection power of 6 dBm.

(B) The NRZ-to-PRZ performance at 9.953 Gbit/s (sonet SDH, OC-192)

A higher data rate can be achieved by raising the DC bias current and reducing the RF modulating power of the FPLD (remaining it at unlasing condition), since the modulating bandwidth is proportional to the DC biased current of FPLD. The highest data rate with BER of 10^{-9} achieved at different DC biased currents is shown as Fig. 3.16. No DC bias current is required for the FPLD to achieve a data rate up to 6 Gbit/s. However, the NRZ-to-PRZ data rate of 9.953 Gbit/s can only be achieved by increasing the DC bias current of the FPLD to 9 mA or larger. The maximum data rate is limited by the carrier lifetime and the DC bias of FPLD.

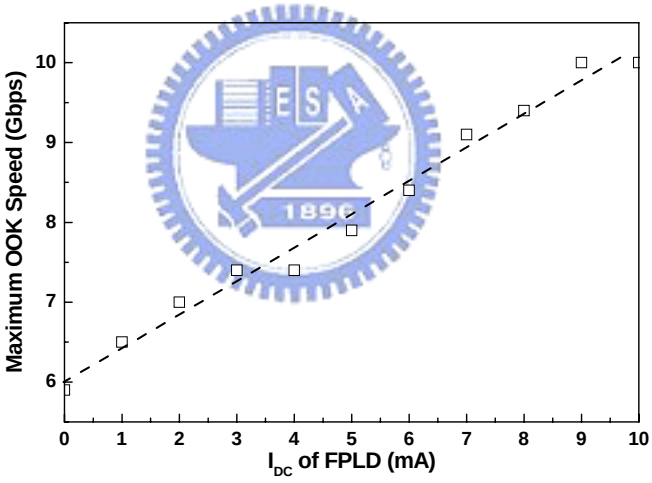

Fig. 3.16 The variation of OOK data rate at different FPLD's DC bias.

Figure 3.17 shows the electrical NRZ data-stream before the MZM, the optical NRZ data-stream after MZM, and the transformed PRZ data-stream generated from the injection-locked and gain-switched FPLD at a sonnet SDH data rate of 9.953 Gbit/s, respectively. An 8-bit edited NRZ pattern 01110101 (Fig. 3.17(a)) is sent into the MZM, and the logically inverted optical NRZ pattern 10001010 is obtained at the MZM output port (Fig. 3.17(b)). The encoded optical data injected into the FPLD for

NRZ-to-PRZ transformation, resulting in a PRZ-format data 10001010, as shown in Fig. 3.17(c). The eye diagrams of the electrical NRZ data-stream before the MZM, the optical NRZ data-stream after MZM, and the transformed PRZ data-stream generated from the injection-locked FPLD are shown in Fig. 3.18(a), (b), and (c), respectively.

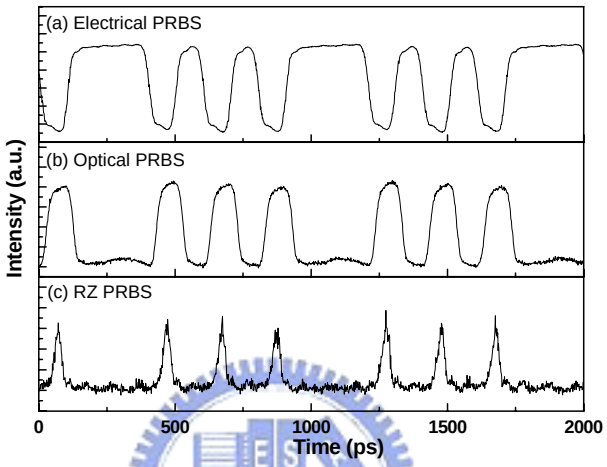

Fig. 3.17 The patterns: (a) the electrical NRZ data before the MZM; (b) the PG-encoded external injection light; (c) the transformed PRZ signal generated from the injection-locked FPLD. The data rate is 9.953 Gbit/s.

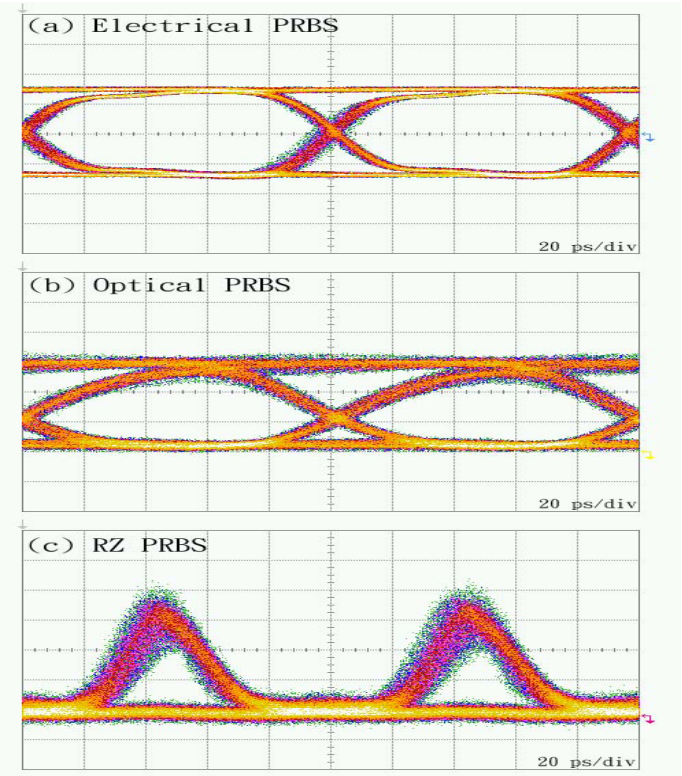

Fig. 3.18 The corresponding eye diagrams: (a) the electrical NRZ data before the MZM; (b) the PG-encoded external injection light; (c) the transformed PRZ signal generated from the single-mode FPLD. The data rate is 9.953 Gbit/s

By externally injecting into the FPLD with a 2^{23}-1 bit PRBS NRZ data-stream at 9.953 Gbit/s, the BER plotted as a function of the receiving optical power for the NRZ-format optical data and the transformed PRZ-format output data are shown in Fig. 3.19. The result shows that the FPLD-based NRZ-to-PRZ data transformer has a power penalty of 1.5 dB at 10^{-9} BER level. An error-free (BER < 10^{-12}) PRZ-format data-stream can be achieved at a receiving optical power as low as -16 dBm.

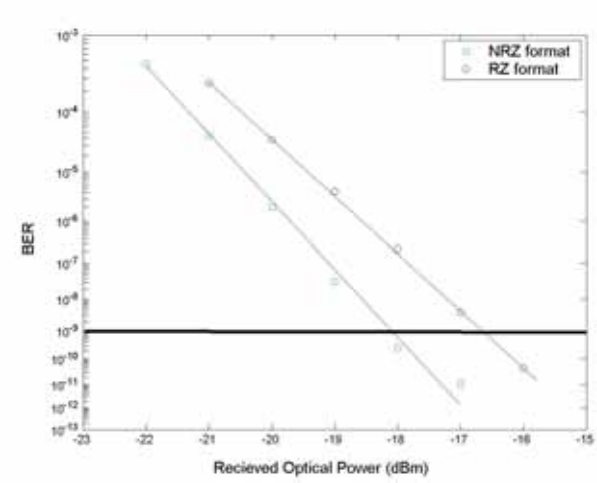

Fig. 3.19 The BER against the received optical power for NRZ-encoded external injection light and transformed PRZ signal at data rate of 9.953 Gbit/s.

When external injection power is larger than 2 dBm, the BER of the PRZ-format data-stream can be as small as 10^{-9} (see Fig. 3.20). Even a BER of 10^{-12} can be observed under an external injection power of 4 dBm.

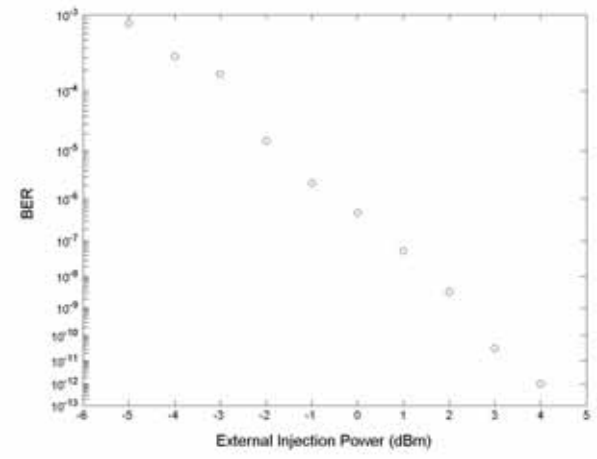

Fig. 3.20 The BERs for different external injection powers at data rate of 9.953 Gbit/s.

Table 3.1 compares the performances among versatile NRZ-to-PRZ techniques. Our proposed system exhibits the better on/off ER of 12.2 dB, the higher SMSR of 40 dB, and the lower BER of 10^{-12} can be achieved. Moreover, the narrowest pulsewidth of 27 ps at data rate of 9.953 Gbit/s can greatly increase the timing tolerance in TDM application. Although the power penalty of 1.5 dB at data rate of 9.953 Gbit/s in our

configuration is less comparable with that proposed using dual-wavelength injection technique (with power penalty of -9.5 dB), such a simple NRZ-to-PRZ transformer still benefits from the advantages of easier operation and low cost.

Table 3.1. Comparison among versatile NRZ-to-PRZ techniques

Mechanism / *Characteristics*	**Dual-wavelength Injection (Hong Kong)**	**Self-phase Modulation (Korea)**	**Single-mode Injection (Taiwan)**
Power penalty	-9.5 dB	NA	1.2 dB (OC-48) 1.5 dB (OC-192)
Maximum ER	12 dB	10.5 dB	12.2 dB
Maximum SMSR	> 30 dB	NA	40 dB
Data rate	3.3 Gbit/s	10 Gbit/s	10 Gbit/s
Operation of FPLD	CW lasing	CW lasing	Unlasing (with below-threshold RF modulation)
Complexity	High	Low	Midium
Pulsewidth	47 ps	30 ps	44 ps (OC-48) 27 ps (OC-192)
Year	2002	2004	2004

3.5 Applications

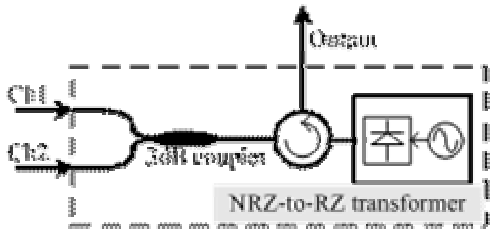

Fig. 3.21 An all-optical logical OR gate by using the NRZ-to-PRZ format transformer.

The last experiment demonstrates an all-optical OR gate operation by using the FPLD-based NRZ-to-PRZ format transformer. The schematic diagram is depicted in Fig. 3.21. The different NRZ data-streams from two channels (Ch1 and Ch2) at same data rate of 2.488 Gbit/s are shown in Fig. 3.22(a) and (b). The incoming data patterns in Ch1 and Ch2 are 10001010 and 10100010, respectively. As a result, the PRZ-output data-stream is 10101010 as shown in Fig. 3.22(c).

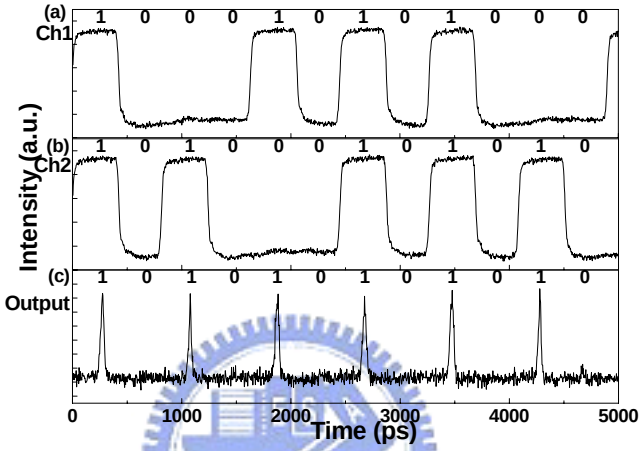

Fig. 3.22 Illustration of the input data (Ch1 and Ch2) and the transformed PRZ signal at data rate of 2.488 GHz.

Similarly, the incoming NRZ data-streams (at data rate of 9.953 GHz) with patterns 01010000 and 01000100 for Ch1 and Ch2, respectively (shown in Fig. 3.23(a) and (b)) leads to a PRZ-output data-stream with pattern of 01010100, as shown in Fig. 3.23(c). The truth table for this all-optical OR-gate logical function is shown in Table 3.2.

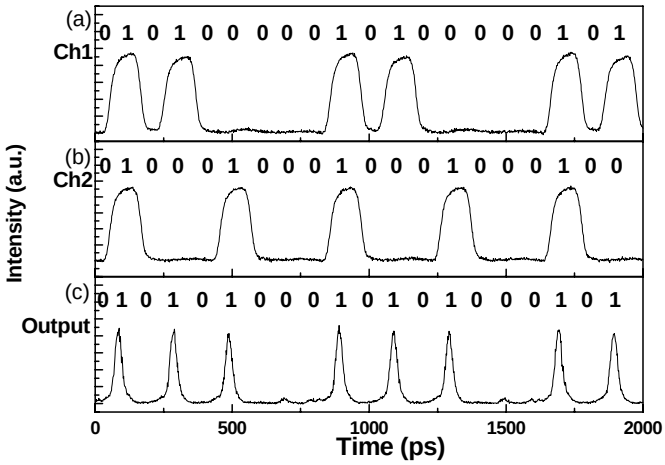

Fig. 3.23 Illustration of the input data (Ch1 and Ch2) and the transformed PRZ signal at data rate of 9.953 GHz

Note that the setting of the RF driving power will influence the stability of this function. The best RF driving power is set at 24.7 dBm for stable operation due to a larger tolerance on the external injection power (see trace (c) in Fig. 3.7), whereas the most unstable operation is observed at a RF driving power of 24.4 dBm (see trace (d) in Fig. 3.7).

Table 3.2. Truth table for all-optical OR operation.

Ch1	Ch2	Output
0	0	0
1	0	1
0	1	1
1	1	1

3.6 Conclusion

We have demonstrated an external-injection power controlled geometry to generate an NRZ-to-PRZ format transformer by biasing the FPLD under unlasing condition. Unlike the mechanisms in [15, 16], the external injection-induced NRZ-to-PRZ transformation is realized by carefully setting the RF driving power approaching but underlying the threshold current. Therefore, under the external light

injection, the FPLD will translate the non-lasing condition into the gain-switching condition. The ERs are 10.5 dB (under wavelength-matched and -mismatched conditions) and 12.2 dB (with and without external injection). In addition, the ER is related with the external injection power and the RF driving power of the FPLD. The maximum ER of 12.2 dB is observed at the RF driving power of 24.4 dBm and the external injection power of -2 dBm. The timing jitter decreases from 0.7 to 0.4 ps and the pulsewidth decreases from 47 to 44 ps with increase of the external injection power. With external injection power of 6 dBm, the gain-switching pulses exhibit relatively low phase noise of -100 dBc/Hz at 5 kHz offset from carrier frequency. By using a pattern generator to simulate the incoming NRZ data, the transformed PRZ data and the corresponding BER are also measured. At data rate of 2.488 GHz (OC-48), the power penalty of 1.2 dB at 10^{-9} BER level is measured in the NRZ-to-PRZ data transformer. Similarly, at data rate of 9.953 GHz (OC-192), the power penalty at 10^{-9} BER level is 1.5 dB. The BER is also influenced by the external injection power. When external injection power is larger than 3 dBm, the BER of the PRZ-format output data can be as small as 10^{-9}. In applications, an optical OR gate is realized by using an NRZ-to-PRZ format transformer with a 3-dB coupler. It is noted that an appropriate RF driving power is needed for the tolerance toward the variation of power of each channel. Such a unit can play both the roles of an all-optical logical OR gate and an NRZ-to-PRZ transformer.

Chapter 4

Summary

First, we theoretically analyze the effect of feedback seeding power for the FPLD on the linewidth, SMSR, and mode-beating noise characteristics of a mutually injection-locked EDFL-FPLD or EDFA-FPLD link. The SMSR and 3-dB linewidth of such a link as a function of feedback power dependent reflectivity change are simulated. By comparing the EDFL-FPLD link with the EDFA-FPLD link, it is found that the side-mode in the EDFL-FPLD link can be entirely eliminated in the EDFA-FPLD link due to the effects of mutual injection-locking, intra-cavity OBPF and active FPLD filtering. To help selecting the strongest mode from the gain spectrum of the FPLD in the EDFA-FPLD link, the FPLD must be biased just below threshold current. In the EDFA-FPLD link, the narrowest 3-dB linewidth of 3.4 MHz and a comparable SMSR of 42 dB with a commercial DFBLD are obtained under a feedback injecting power of 5.4 mW. The maximum output power of the current EDFA-FPLD link is limited at 20 mW, and the improvement relies on the use of an FPLD with larger output power.

On the other hand, all optical format conversion of NRZ into a PRZ data stream is demonstrated by using a synchronously modulated Fabry-Perot laser diode (FPLD) just below threshold current. The NRZ-to-PRZ transformation is implemented by gain-switching the FPLD injected externally by an optical NRZ data stream. The optimized RF driving power of the FPLD is ranged between 24.4 dBm and 24.7 dBm. The on/off extinction ratio and side mode suppression ratio of the FPLD based data transformer are severely dependent on external injecting wavelength and power. At optimized injecting power of -2 dBm, the maximum ER and SMSR of the injection-locked FPLD are up to 12.2 dB and 40 dB when the injecting wavelength is

coincident well with some FPLD's longitudinal mode. Linewidth broadening of injection-locked FPLD from 0.04 to 0.19 nm at 10-dB decay is also observed at mode matching condition. The smallest timing jitter and narrowest pulsewidth of the gain-switched PRZ pulses from FPLD are 0.4 ps and 44 ps, respectively. With the received optical power and external injecting power of larger than -22 dBm and 6 dBm, respectively, the BER of the PRZ data-stream at 2.488 Gbit/s can be smaller than 10^{-12}. The power penalty of the FPLD based NRZ-to-PRZ data transformer can be smaller than 1.2 dB at a BER of 10^{-9}. By increasing DC-biased current of the FPLD, the maximum NRZ-to-PRZ conversion rate of the FPLD can be up to 9.953 Gbit/s with a power penalty of 1.5 dB at a BER of 10^{-9}. In application, an all-optical OR gate is realized by using the FPLD-based NRZ-to-PRZ format transformer with a 3-dB coupler.